AGU PUBLICATIONS

Global Biogeochemical Cycles

RESEARCH ARTICLE
10.1002/2017GB005655

Key Points:
- $^{13}CH_3D$ is expected to trace atmospheric methane sources
- $^{12}CH_2D_2$ is expected to trace both atmospheric methane sources and sinks
- The reactions of methane with •OH and Cl• generate a distinct signature of higher $\Delta^{12}CH_2D_2$ relative to the source composition

Supporting Information:
- Supporting Information S1

Correspondence to:
M. A. Haghnegahdar,
mojhganhagh@ucla.edu

Citation:
Haghnegahdar, M. A., E. A. Schauble, and E. D. Young (2017), A model for $^{12}CH_2D_2$ and $^{13}CH_3D$ as complementary tracers for the budget of atmospheric CH_4, *Global Biogeochem. Cycles*, *31*, doi:10.1002/2017GB005655.

Received 24 FEB 2017
Accepted 24 JUL 2017
Accepted article online 27 JUL 2017

A model for $^{12}CH_2D_2$ and $^{13}CH_3D$ as complementary tracers for the budget of atmospheric CH_4

Mojhgan A. Haghnegahdar[1], Edwin A. Schauble[1], and Edward D. Young[1]

[1]Department of Earth, Planetary, and Space Sciences, University of California, Los Angeles, California, USA

Abstract We present a theoretical model to investigate the potential of $^{13}CH_3D$ and $^{12}CH_2D_2$, the doubly substituted mass-18 isotopologues of methane, as tools for tracking atmospheric methane sources and sinks. We use electronic structure methods to estimate kinetic isotope fractionations associated with the major sink reactions of methane in air (reactions with OH and Cl radicals) and combine literature data with reconnaissance measurements of the relative abundances of $^{13}CH_3D$ and $^{12}CH_2D_2$ to estimate the compositions of the largest atmospheric sources. This model atmospheric budget is investigated with a simplified box model in which we explore both steady state and dynamical (nonsteady state) conditions triggered by changes in emission or sink fluxes. The steady state model predicts that sink reactions will generate a marked (>100‰) clumped isotope excess in atmospheric $\Delta^{12}CH_2D_2$ relative to the net source composition. $^{12}CH_2D_2$ measurements may thus be useful for tracing both atmospheric source and sink fluxes. The effect of sinks on $\Delta^{13}CH_3D$ is much less pronounced, indicating that $^{13}CH_3D$ in air will give a more focused picture of the source composition.

1. Introduction

In this study we develop a theoretical model using the relative abundances of $^{13}CH_3D$ and $^{12}CH_2D_2$, the doubly substituted mass-18 isotopologues of methane, to quantitatively track the sources and the sinks of atmospheric methane. The ultimate goal is to develop new tracers for atmospheric methane.

Atmospheric methane is the second most important long-lived greenhouse gas in Earth's atmosphere; it contributes 0.5 W m^{-2} to total radiative forcing [*Dlugokencky et al.*, 2011; *Intergovernmental Panel on Climate Change (IPCC)*, 2013]. Moreover, as the result of reactions with radicals in the atmosphere it plays an important role in producing tropospheric ozone and stratospheric water vapor. This indirectly adds around 0.2 W m^{-2} to its forcing [*Dlugokencky et al.*, 2011; *IPCC*, 2013]. Natural sources of methane include wetlands, oceans, termites, and the breakdown of clathrates, whereas major anthropogenic sources include fossil fuel exploitation, ruminant livestock, rice agriculture, waste management, and biomass burning. Biogenic generation and thermogenic generation of methane are both significant [*Wuebbles and Hayhoe*, 2002].

The methane concentration in the atmosphere increased through much of the twentieth century, reaching 1.7 ppmv in 1990 [*Dlugokencky et al.*, 1994; *Bréas et al.*, 2001], then leveled off from 1990 until 2007 [*Rigby et al.*, 2008]. The rise has now resumed. Since 2007, the global average growth of methane concentration has been ~6 ppb/yr [*Kirschke et al.*, 2013]. However, the mechanism and origin of this new upward trend are not fully understood [*Rigby et al.*, 2008; *Dlugokencky et al.*, 2011; *Montzka et al.*, 2011; *Bousquet et al.*, 2011; *Kirschke et al.*, 2013]. Possibilities include enhanced wetland CH_4 emission, anthropogenic CH_4 emissions, wild fires, less intense OH photochemistry, and interannual wind changes. More generally, there is a lack of understanding regarding the factors that have driven the rise in methane concentrations during the past few decades [*IPCC*, 2013], highlighting uncertainties in the methane atmospheric budget [*Bousquet et al.*, 2011; *Dlugokencky et al.*, 2011; *Kirschke et al.*, 2013; *IPCC*, 2013]. Inverse (top-down) models of the methane budget are not consistent with process-based (bottom-up) models and inventories. Identifying the role of sinks as well as sources should improve our overall understanding of the atmospheric methane budget.

Isotopic measurements have been a valuable tool for distinguishing among various sources of CH_4 to the atmosphere [*Cicerone and Oremland*, 1988; *Dlugokencky et al.*, 2011]. The $\delta^{13}C$ and (less commonly) δD measurements of atmospheric methane have been reported in numerous studies [*Wilmshurst and Bernstein*, 1957; *King et al.*, 1989; *Fung et al.*, 1991; *Levin et al.*, 1993; *Hein and Crutzen*, 1997; *Lowe et al.*, 1999;

Quay et al., 1999; *Bréas et al*., 2001; *Saueressig et al*., 1995, 2001; *Fletcher et al*., 2004; *Whiticar and Schaefer*, 2007]. Different methane sources have different $^{13}C/^{12}C$ and D/H ratios, depending on the methane formation process and the carbon and hydrogen isotope compositions of precursor materials [*Cicerone and Oremland*, 1988]. In general, methane produced at high temperatures, including methane released from biomass burning or natural gas, is enriched in both ^{13}C and D [*Cicerone and Oremland*, 1988] relative to low-temperature methane sources. However, $^{13}C/^{12}C$ and D/H do not always uniquely resolve methane originating from microbial, thermogenic, and abiotic sources. [*Sherwood Lollar et al*., 2006; *Ono et al*., 2014; *Stolper et al*., 2014a]. Precise analyses of doubly substituted methane isotopologues (clumped isotopes) may offer additional constraints on methane sources [*Ma et al*., 2008; *Stolper et al*., 2014a; *Wang et al*., 2015; *Young et al*., 2016, 2017].

Atmospheric sink reactions are slower for D-substituted methane isotopologues [*Alei et al*., 1987; *Cicerone and Oremland*, 1988; *Mroz et al*., 1989], resulting in higher D/H in air compared to most sources. Methane containing multiple deuterium atoms (e.g., $^{12}CD_4$) has been analyzed in the atmosphere and found in much higher concentrations than would be expected from likely sources, suggesting a strong signature of sink reaction kinetics [*Mroz et al*., 1989; *Kaye and Jackman*, 1990]. More recently, precise measurements of $^{13}CH_3D$ have been tested as potential tools for determining the generation temperature and mechanism for different sources of methane [*Stolper et al*., 2014a, 2014b; *Wang et al*., 2015]. *Douglas et al*. [2016] used Δ_{18} methane (departures in the relative abundances of both mass-18 isotopologues from the stochastic distribution) as a tool to determine the source of natural methane emissions from Arctic and sub-Arctic. *Tsuji et al*. [2012] performed spectroscopic isotope measurements on $^{13}CH_3D$ to determine the isotope ratios of $^{13}CH_3D/^{12}CH_3D$ and $^{13}CH_3D/^{12}CH_4$ in natural methane. *Young et al*. [2017] obtained both $^{13}CH_3D/^{12}CH_4$ and $^{12}CH_2D_2/^{12}CH_4$ signatures of abiotic and biotic methane formation in natural settings and in the laboratory. Theoretical studies of the equilibrium distribution of $^{13}CH_3D$ [*Cao and Liu*, 2012; *Webb and Miller*, 2014] and $^{12}CH_2D_2$ [*Stolper et al*., 2015; *Young et al*., 2016, 2017; *Piasecki et al*., 2016] have also appeared. The $^{13}CH_3D/^{12}CH_4$ kinetic isotope effects in the sink reaction with Cl and OH radicals were determined for the first time by *Joelsson et al*. [2014, 2016] using Fourier transform infrared (FTIR) spectroscopy. Kinetic isotope effects for $^{12}CH_2D_2$ in reactions with OH and Cl radicals have also been measured [*Gierczak et al*., 1997; *Sauer et al*., 2015; *Feilberg et al*., 2005; *Boone et al*., 2001; *Matsumi et al*., 1997; *Wallington and Hurley*, 1992].

In the present study, we investigate the potential for using two doubly substituted methane isotopologues, $^{13}CH_3D$ and $^{12}CH_2D_2$, as tracers of atmospheric methane cycling. There are no existing models, to our knowledge, that consider $^{13}CH_3D$ and $^{12}CH_2D_2$ in concert as distinct species for atmospheric studies. In the present work, we use electronic structure methods to estimate kinetic and equilibrium isotope signatures for methane sink reactions, including both mass-18 doubly substituted isotopologues of methane. We use our results to model the relative abundances of singly and doubly substituted methane species in the atmosphere in different relevant scenarios in order to assess the utility of the multiply substituted species as tracers.

2. Methods

2.1. First-Principles Calculations of Isotope Partitioning

We use first-principles electronic structure calculations to estimate kinetic and equilibrium isotope effects. All electronic structure calculations are made with the Gaussian 09 software package (EM64L-G09RevD.01 [*Frisch et al*., 2013]). The main results reported in this study are based on second-order Møller-Plesset theory (MP2 [*Møller and Plesset*, 1934]) and the medium-sized Gaussian basis sets cc-pVTZ [*Dunning*, 1989]. We also tried 6-311G** [*Krishnan et al*., 1980] basis sets to test for consistency. These model chemistries do well at reproducing previous measurements and high-precision theoretical calculations of structural and vibrational properties of methane. No frequency scale factor or correction for anharmonicity has been used for our calculations and comparisons. Table 1 presents the comparison between our calculated harmonic frequencies of methane (cm^{-1}) and those of previous studies [*Gray et al*., 1979; *Lee et al*., 1995; *Liu and Liu*, 2016]. Harmonic frequencies for all isotopologues are in Table S1 in the supporting information. Kinetic isotope effects ($KIE = \frac{k_{CH4}}{k_i}$) for sink reactions with OH and Cl radicals are modeled using transition state theory, with a one-dimensional Wigner tunneling correction for hydrogen and

Table 1. Comparison of Harmonic Frequencies (cm^{-1}) for $^{12}CH_4$ Between the Present Study and Previous Works[a]

	Present Work	*Liu and Liu* [2016]	*Lee et al.* [1995]	*Gray et al.* [1979]	*Bottinga* [1969]	*Jones and McDowell* [1959] (Recalculated)
Mode	MP2/cc-pVTZ	CCSD/aug-cc-pVTZ	CCSD(T)/cc-pVQZ	Expt./FF	Expt./FF	Expt./FF
A_1	3076	3045	3036	3026	3143	3143
E	1586	1584	1570	1583	1573	1573
F_2 stretch	3212	3162	3157	3157	3154	3154
F_2 bend	1350	1363	1345	1367	1357	1358
RMS error versus G&R 1979	38	10	14	–	59	59
Mean error versus G&R 1979	23	5	−6	–	24	24
$10^3 \ln[K_{eq}(^{13}CH_3D)]$	5.78	5.73	5.71[b]	5.73[b]	5.82[c]	5.69[b]
$(8/3)\ 10^3 \ln[K_{eq}(^{12}CH_2D_2)]$	19.49	–	19.06[c], 19.20[b]	20.49[c], 19.72[b]	20.42[c]	19.67[b]

[a](*G&R*, 1979 refers to *Gray et al.* [1979])
[b]K_{eq} determined using frequencies recalculated with tabulated force field.
[c]K_{eq} calculated from tabulated vibrational frequencies (correcting for an apparent data entry error in the original *Gray et al.* [1979], tabulation)

deuterium [*Gupta et al*., 1997]. Test calculations indicate that tunneling of H-atoms is significant for absolute rate constants and KIEs in both sink reactions (Table S2). In both reactions, corrected KIEs for $^{12}CH_3D$ and $^{12}CH_2D_2$ are about 0.1 larger than noncorrected values. We use Harmonic vibrational frequencies in transition state calculations. Saddle-point and reactant geometries are fully (energy) optimized at each level of theory. *Lasaga and Gibbs* [1991], *Gupta et al*. [1997], *Truong and Truhlar* [1990], *Tanaka et al*. [1996], and *Roberto-Neto and Coitin* [1998] used similar approaches to estimate KIEs of the reaction of singly substituted CH_4 isotopologues with •OH and Cl•, yielding results similar to those of the present study. The optimized geometries for both reactions are given in Table 2. Figure 1 shows the transition state of methane in reaction with •OH and Cl•. Harmonic frequencies for both transition states are in Table S3.

Equilibrium abundances of isotopologues are calculated using harmonic vibrational frequencies, based on the following exchange reactions and associated equilibrium constants:

$$^{13}CH_4 + {}^{12}CH_3D \rightleftharpoons {}^{12}CH_4 + {}^{13}CH_3D \quad (1)$$

$$K_{eq} = \frac{[^{13}CH_3D][^{12}CH_4]}{[^{13}CH_4][^{12}CH_3D]} \quad (2)$$

and

$$2\,{}^{12}CH_3D \rightleftharpoons {}^{12}CH_4 + {}^{12}CH_2D_2 \quad (3)$$

$$K_{eq} = \frac{[^{12}CH_2D_2][^{12}CH_4]}{[^{12}CH_3D]^2} \quad (4)$$

These equilibrium constants are sensitive to temperature, with $K_{eq}(^{13}CH_3D) \approx 1.007$ and $K_{eq}(^{12}CH_2D_2) \approx 1.02 \times (3/8)$ at ambient conditions ~300 K, where $K_{eq}(^{12}CH_2D_2) = 3/8$ represents the stochastic distribution of isotopologues.

Table 2. The Optimized Geometries of Transition State Structures of Methane Reactions With OH and Cl Radicals[a]

OH

C——H 1.083 Å C------H 1.189 Å O------H 1.317 Å O——H 0.9677 Å

Cl

C——H 1.080 Å C------H 1. 359 Å Cl------H 1.451 Å

[a]Bonds directly participating in the reaction are indicated by dotted lines.

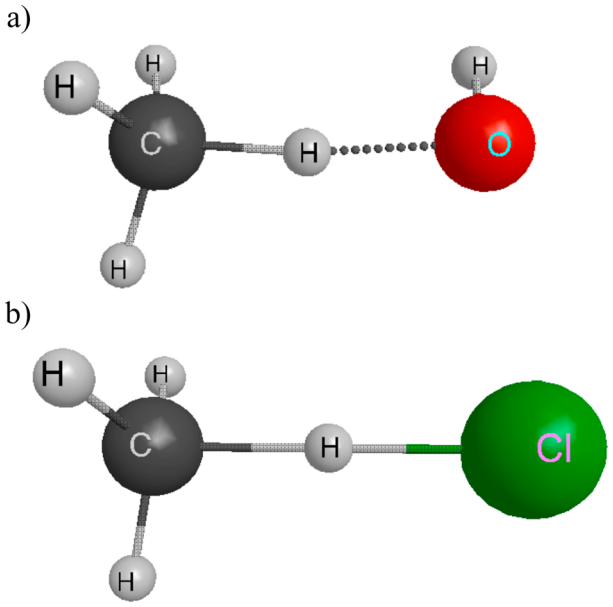

Figure 1. Transition state structures for (a) CH_4---•OH and (b) CH_4---Cl• sink reactions determined by electronic structure calculations at the MP2/cc-pVTZ level.

Isotopic distributions for clumped isotope species are expressed in delta notation:

$$\delta^i = \left(\frac{{}^iR_{\text{sample}}}{{}^iR_{\text{standard}}} - 1\right)(1000‰) \quad (5)$$

$$\Delta_j = \left(\frac{{}^{ij}R_{\text{sample}}}{{}^{ij}R_{\text{stochastic}}} - 1\right)(1000‰) \quad (6)$$

where R represents abundance ratios $^{13}CH_3D/^{12}CH_4$ or $^{12}CH_2D_2/^{12}CH_4$ for a sample, standard, or stochastic equivalent. D/H and $^{13}C/^{12}C$ ratios for the stochastic reference for each gas are calculated solely from the abundance ratios $^{12}CH_3D/^{12}CH_4$ and $^{13}CH_4/^{12}CH_4$, i.e., D/H = 1/4($^{12}CH_3D/^{12}CH_4$) and $^{13}C/^{12}C = {}^{13}CH_4/^{12}CH_4$. This treatment neglects the effects of nonstochastic isotopologue partitioning on the abundances of singly substituted species; however, numerical tests show no significant loss in accuracy in using this approach to determine bulk isotope ratios for gases, within the likely natural range of isotopologue distributions.

2.2. Atmospheric Methane Budget

We construct a model for steady state $^{13}CH_3D$ and $^{12}CH_2D_2$ abundances in the atmosphere by considering the isotope and isotopologue compositions of major methane sources and isotope fractionations associated with the major sink reactions; the reactions of methane with OH and Cl radicals are the main sinks for atmospheric methane and are assumed to be the only fractionating sinks in our model. The model considers $\Delta^{13}CH_3D$ and $\Delta^{12}CH_2D_2$ of atmospheric methane in a homogenous "troposphere" reservoir, controlled by a balance between the emission flux of different sources to the atmosphere and the rates of CH_4 destruction by reaction with •OH and Cl•. We also designed a box model to investigate nonsteady state scenarios by inducing imbalances and changes in emissions and sinks.

2.2.1. Atmospheric Sources and Isotopologue Abundances

There are significant uncertainties in the estimated fluxes of individual methane sources as well as the overall global budget. Here we use a "bottom-up" budget proposed by *Whiticar and Schaefer* [2007]. In this model, the total methane flux is 540 Tg/yr. The leading methane emission sources to the atmosphere are biogenic, including wetlands, rice paddies, ruminants, landfills, aerobic methane production (AMP), termites, oceans, and fresh water (Table 3). Wetlands, with a flux of 115 Tg/yr, are the most important source category. Abiogenic methane sources include natural gas, biomass burning, coal, gas hydrates, and geological. Among these sources, biomass burning and coal have the highest fluxes with 41 Tg/yr and 35 Tg/yr, respectively (Table 3) [*Whiticar and Schaefer*, 2007]. In this group, AMP is perhaps the most controversial component—it is not included in some other recent source budgets, and estimates of the size of this source vary widely [*Kirschke et al*., 2013; *Saunois et al*., 2016]. However, AMP makes up a minor part of the total assumed biogenic methane source, and we assume that it has isotope signatures similar to microbial methane sources. The inclusion of AMP in our model budget does not substantially affect our overall conclusions. Aside from AMP, wetland emissions show the largest uncertainties, especially in the direction of higher emission, with more recent top-down estimates ranging from 142 to 208 Tg/yr and bottom-up estimates ranging from 177 to 284 Tg/yr [*Kirschke et al*., 2013]. For biomass burning, top-down source estimates are ranging from 24 to 45 Tg/yr, while bottom-up calculations suggest a range of 32 to 39 Tg/yr [*Kirschke et al*., 2013]. For fossil fuels (including coal) top-down estimates range from 77 to 123 Tg/yr and bottom-up estimates range from 85 to 105 Tg/yr [*Kirschke et al*., 2013].

The $\delta^{13}CH_3D$, $\delta^{12}CH_2D_2$, $\Delta^{13}CH_3D$, and $\Delta^{12}CH_2D_2$ values for each major atmospheric methane source are estimated by combining the *Whiticar and Schaefer* [2007] results for total fluxes and bulk isotopic compositions

Table 3. Atmospheric Source Models, Including Calculated $\Delta^{13}CH_3D$ and $\Delta^{12}CH_2D_2$ Values, for Atmospheric Methane Sources and Air, Based on the Pseudo-Equilibrium Model (pEM), the *Stolper et al.* [2015] Model Predictions (SMC-15), and a Disequilibrium Model Based on Reconnaissance $\Delta^{12}CH_2D_2$ Measurements (DM) ($\delta^{13}C$ and δD Values From *Whiticar and Schaefer* [2007] and *Quay et al.* [1999])

Source	Flux (Tg/yr)	$\delta^{13}CH_4$ (‰)	δD-$^{12}CH_4$ (‰)	$\delta^{12}CH_2D_2$ (‰)	$\delta^{13}CH_3D$ (‰)	T (K)	$\Delta^{13}CH_3D$ pEM and SMC-15 (‰)	$\Delta^{12}CH_2D_2$ pEM (‰)	$\Delta^{12}CH_2D_2$ Stolper SMC-15 (‰)	$\Delta^{12}CH_2D_2$ Young DM (‰)	$\Delta^{13}CH_3D$ Young DM (‰)
Rice paddies	110	−63	−320	−528.8	−359.2	302	5.65	19.14	19.14	19.14	
Ruminants	80	−60.5	−330	−549.7	−369.5	585	1.59	3.04	20.00	−31.4	−0.64
Natural gas	45	−44	−180	−322.5	−213.7	433	2.98	7.57	7.57	7.57	
Coal	35	−37	−140	−254.8	−169.4	433	2.98	7.57	7.57	7.57	
Biomass burning	41	−24.6	−225	−394.83	−241.8	433	2.98	7.57	7.57	7.57	
Boreal wetlands	38	−62	−380	−607.2	−414.87	285	6.22	21.87	21.87	21.87	
Tropical wetlands	77	−58.9	−360	−582	−394.1	293	5.94	20.49	20.49	20.49	
Termites	16	−63	−390	−620.3	−425	293	5.94	20.49	20.49	20.49	
Landfills	40	−55	−310	−522.5	−346.9	585	1.59	3.04	20.00	−31.4	−0.64
Ocean	10	−58	−220	−379.1	−260.9	293	5.94	20.49	20.49	20.49	
Fresh water	4	−53.8	−385	−614.5	−414.8	302	5.65	19.14	19.14	19.14	
Gas hydrates	4	−62.5	−190	−338.9	−238.4	433	2.98	7.57	7.57	7.57	
Geological	0	−41.8	−200	−355.2	−231.2	433					
AMP	40	−51.2	−260	−450.7	−296.8	585	1.59	3.04	20.00	−31.4	−0.64
Calculated total source	540	−54.2	−295	−492.8	−330.4	253	4.76	21.70	26.57	11.83	4.11
Measured CH_4 in air	540	−47.1	−86	?	?		?	?			

with the $^{13}CH_3D$ measurements of *Young et al.* [2017], *Stolper et al.* [2015], *Wang et al.* [2015], our own theoretical calibration of the $^{12}CH_2D_2$ equilibrium, and initial $^{12}CH_2D_2$ measurements at University of California Los Angeles (UCLA) [*Young et al.*, 2017]. The $\delta^{13}C$ and δD values for the source terms combined are calculated according to

$$\delta = \frac{\Sigma_i E_i \delta_i}{\Sigma_i E_i} \tag{7}$$

where δ_i is either $\delta^{13}C$ or δD for source i in ‰ and E_i is the flux of the source i in Tg/yr.

The abundances of doubly substituted isotopologues in major atmospherice methane sources are not well known, though some individual sample measurements that may be representative of source components are now available [*Stolper et al.*, 2015; *Wang et al.*, 2015; *Young et al.*, 2017]. It is therefore necessary to make assumptions about some components to assemble a complete budget. Our basic approach is to assume that nonmicrobial source components form in internal isotopic equilibrium at temperatures characteristic of the methane formation process; this assumption is consistent with initial measurements of $^{13}CH_3D$ by *Stolper et al.* [2014b] and *Wang et al.* [2015]. However, measurements of $\Delta^{13}CH_3D$ in biogenic methane indicate that these sources tend not to show low-T equilibrium (i.e., $\Delta^{13}CH_3D \geq 5‰$) but are instead closer to stochastic ($\Delta^{13}CH_3D < 5‰$ [*Wang et al.*, 2015]). Furthermore, initial measurements at UCLA of $\Delta^{13}CH_3D$ and $\Delta^{12}CH_2D_2$ in microbially produced methane in the laboratory yield significant deficits in $\Delta^{12}CH_2D_2$ relative to equilibrium. We therefore use these microbial $\Delta^{13}CH_3D$ and $\Delta^{12}CH_2D_2$ measurements to represent biogenic atmospheric sources in our primary budget. Whether these reconnaissance measurements accurately represent natural systems remains to be seen, however, and it appears that microbial communities can cycle or produce methane with either equilibrium or disequilibrium isotopologue abundances depending upon rates of processing

[e.g., *Wang et al*., 2015; *Young et al*., 2017]. To investigate this possibility, we have constructed an alternative budget by assuming an effective equilibrium at a "temperature" of 300°C for $\Delta^{13}CH_3D$ and $\Delta^{12}CH_2D_2$ for biogenic methane, roughly matching the $\Delta^{13}CH_3D$ measurements of *Wang et al*. [2015]. Finally, we have constructed a third possible budget using the biogenic sample $\Delta^{13}CH_3D$ measurements of *Stolper et al*. [2015], along with model biogenic source $\Delta^{12}CH_2D_2$ compositions predicted by that study. These three alternative source budgets will be referred to as DM (disequilibrium model), pEM (pseudo-equilibrium model), and SMC-15 (*Stolper et al*. [2015] measurements and model). By considering these alternatives we are able to get a sense of how important biogenic source compositions are for the total atmospheric source isotopologue budget (Table 3). Reference bulk isotope ratios are taken to be $(^{13}C/^{12}C)_{VPDB}$ = 0.0112372 [*Assonov and Brenninkmeijer*, 2003] and $(D/H)_{VSMOW}$ = 1.5576 × 10^{-4} [*Schimmelmann et al*., 2006].

In the discussion that follows, it will be useful to remember that δ values for $^{13}CH_3D$ or $^{12}CH_2D_2$ of air can be calculated applying equation (7) for each isotopologue, i.e., that δ values mix in a nearly linear fashion. In contrast, Δ values are not conserved and do not necessarily follow linear mixing trends because the stochastic reference frame changes with the isotopic composition of the gas. The $\Delta^{13}CH_3D$ and $\Delta^{12}CH_2D_2$ in the aggregate atmospheric source are not weighted averages of the $\Delta^{13}CH_3D$ and $\Delta^{12}CH_2D_2$ in individual sources. This property of Δ in isotopologues has been pointed out in previous studies [*Eiler and Schauble*, 2004; *Eiler*, 2007; *Stolper et al*., 2015; *Young et al*., 2017]. In the current study it will become particularly important when comparing closed-system Rayleigh evolution to open-system steady state models of the atmosphere, in which $\Delta^{12}CH_2D_2$ trends in opposite directions from the source composition. The distinct behavior of $\Delta^{13}CH_3D$ in closed systems versus open systems is also reported by *Whitehill et al*. [2017].

2.2.2. Atmospheric Sinks and Kinetic Isotope Effects

The primary sink of atmospheric methane is •OH (90%); reactions with Cl• in the stratosphere and the marine boundary are responsible for an additional ~6% [*Lelieveld et al*., 1998; *Kirschke et al*., 2013] (about 3.3% happening in MBL (marine boundary layer) [*Platt et al*., 2004]). The remaining sinks include soil reactions [*Kirschke et al*., 2013]. There is also a small loss due to reaction with $O(^1D)$, mostly occurring in the stratosphere [*Sauer et al*., 2015].

Kinetic isotope effects of singly substituted methane isotopologues in the •OH and Cl• reactions are known to lead to large (~200‰) D/H and minor (~5‰) $^{13}C/^{12}C$ enrichments in air [e.g., *Lasaga and Gibbs*, 1991; *Saueressig et al*., 1995; *Roberto-Neto and Coitin*, 1998; *Gola et al*., 2005; *Sellevåg et al*., 2006; *Michelsen*, 2001]. The actual fractionations depend to some degree on temperature and on the radical reactant. To simplify the atmospheric steady state model, we have assumed that tropospheric radical reactions determine the atmospheric isotopologue abundances. We assume that ~96.6% of the total methane sink is due to reaction with •OH and the remaining ~3.4% by reaction with Cl•, closely matching the tropospheric •OH/Cl• sink reaction rate of *Kirschke et al*. [2013] while ignoring other minor sink processes. We calculated kinetic isotope effects for both the •OH and Cl• reactions for $^{13}CH_4$, $^{12}CH_3D$, $^{13}CH_3D$, and $^{12}CH_2D_2$.

In order to evaluate possible changes in rare isotopologues of methane during recent changes in atmospheric methane concentration, we constructed a one-box model that allows us to evaluate different scenarios, for instance, by imposing sudden or gradual changes in source and sink rates. We use the rate constants of methane reactions with •OH and Cl• from *Sander* [2006] and apply our estimated kinetic isotope effects to scale the rate constants for each isotopologue. Atmospheric concentrations of •OH and Cl• were also held constant for all scenarios except where we investigated changes in •OH concentration. We use the •OH concentration estimates suggested by *Singh et al*. [1996], *IPCC* [2001], and *Bousquet et al*. [2005]. For Cl•, we obtained our value using the mean concentration suggested by *Allan et al*. [2007] for MBL atomic Cl, scaled to an average tropospheric concentration [*Singh et al*., 1996]. This yields •OH and Cl• concentrations of 10^6 molecule cm^{-3} and 1500 molecule cm^{-3}, respectively. In general, for each radical, we picked a concentration within the suggested range [*Prather*, 1990; *Singh et al*., 1996; *Bousquet et al*., 2005] such that the destruction ratio was in reasonable agreement with *Kirschke et al*. [2013]. In our box models the •OH sink reaction is considered to be occurring at 262 K, the reported effective temperature for this reaction in the troposphere [*Prather*, 1990]. For Cl• reaction with methane the temperature is considered to be 273 K, since the reaction is thought to be most vigorous in the MBL (marine boundary layer).

The basic mass balance equation in all cases is

$$\frac{dn}{dt} = E - kn, \tag{8}$$

where n refers to the moles of the species of interest, E refers to $\sum E_i$ where E_i are fluxes of all the sources, and $k = k_{OH}[OH] + k_{Cl}[Cl]$. The solution to (8) is

$$n(t) = n_0 e^{-kt} + \frac{E}{k}\left(1 - e^{-kt}\right). \tag{9}$$

Steady state solutions can also be obtained from equation (9) in the limit of infinite time (effectively reached on a timescale of hundreds of years).

A gradual (exponential) increase in the overall source term leads to the differential equation:

$$\frac{dn}{dt} = E_0 e^{rt} - kn \tag{10}$$

with the solution

$$n(t) = \left(n_0 - \frac{E_0}{k+r}\right)e^{-kt} + \frac{E_0}{k+r}e^{rt} \tag{11}$$

where r is the rate constant for the changing the source term. For the case of gradual changes in a specific emission source component, the equation becomes

$$\frac{dn}{dt} = E_p + E_s e^{rt} - kn \tag{12}$$

where E_s is the changing source component and E_p represents the unchanging source components. The solution to this equation is

$$n(t) = \frac{E_p}{k} + \frac{E_s}{k+r}e^{rt} + \left(n_0 - \frac{E_p}{k} - \frac{E_s}{k+r}\right)e^{-kt}. \tag{13}$$

We also consider seasonal cycles where the mass balance equation becomes periodic,

$$\frac{dn}{dt} = E_p + E_s \sin 2\pi t - kn, \tag{14}$$

resulting in the time-dependent expression

$$n(t) = \frac{E_p}{k} + e^{-kt}\left(n_0 - \frac{E_p}{k} - \frac{E_s(-2\pi)}{k^2 + 4\pi^2}\right) + \frac{E_s[-2\pi\cos(2\pi t) + k\sin(2\pi t)]}{k^2 + 4\pi^2}. \tag{15}$$

In equation (15) the seasonal cycles are represented by the sinusoidal term $\sin(2\pi t)$, with a period of 1 year. In our calculations the initial steady state residence time for methane in the atmosphere is 10.9 years. This is consistent with recent reported values of 11.2 ± 1.3 years, with respect to reaction with tropospheric hydroxyl radicals [*IPCC*, 2013]. Applying our estimated KIE values, lifetimes for $^{13}CH_4$, $^{12}CH_3D$, $^{13}CH_3D$, and $^{12}CH_2D_2$ in the atmosphere are 11.0, 14.6, 14.7, and 21.5 years, respectively. The wide variation in mean lifetime among different isotopologues leads to complex patterns of variation in isotopologue abundance ratios in non-steady state models, including the simple box model results presented below.

3. Results and Discussion

3.1. Isotope Exchange Equilibrium and Kinetic Isotope Effects

Calculated equilibrium constants for exchange reactions involving singly and doubly substituted isotopologues are shown in Figure 2. The present results for $^{13}CH_3D$ formation agree well with previous studies, including *Webb and Miller* [2014], *Stolper et al*. [2015], and *Liu and Liu* [2016]. They also agree with a recent empirical calibration [*Wang et al*., 2015] within measurement uncertainties. Our calculated $1000\ln(K_{eq})$ at 300 K is 5.78. *Webb and Miller* [2014], using Path Integral Monte Carlo and Urey-HO methods based on high-accuracy electronic structure methods, report values of 5.73 and 5.71, respectively. These same equilibrium constants calculated by *Liu and Liu* [2016], using harmonic and anharmonic methods, are 5.76 and 5.81, respectively. The calculated $1000\ln(K_{eq})$ for $^{12}CH_2D_2$ formation is considerably larger, 19.49 at 300 K. Estimated equilibrium

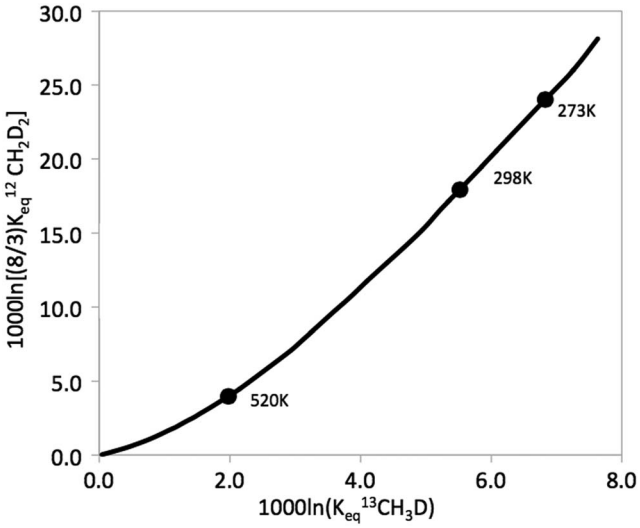

Figure 2. Equilibrium relationship between clumping equilibria for $^{12}CH_2D_2$ and $^{13}CH_3D$, determined at the MP2/cc-pVTZ level.

constants for $^{13}CH_3D$ and $^{12}CH_2D_2$ at the same temperature (5.72 and 19.21, respectively) were reported by *Young et al.* [2016] based on hybrid density functional theory. *Piasecki et al.* [2016] reported estimates of 5.68 and 20.17, respectively, using similar modeling methods. *Stolper et al.* [2015] estimated a 1000ln(K_{eq}) value of 20.42 for this exchange using harmonic vibrational frequencies tabulated by *Bottinga* [1969] based on empirical force field model calculations. A simple comparison of harmonic frequencies from our model, *Bottinga* [1969], and other ab initio and empirical results from the literature does not obviously point to large systematic differences in frequencies (Table 1). One possible reason for the different calculated K_{eq} values is that the frequencies tabulated by *Bottinga* [1969] are rounded to the nearest 0.1 cm^{-1}. Test calculations using that data set indicate that rounding errors of up to ±0.05 cm^{-1} are likely to induce artifacts of several tenths per mil (at ~300 K) in calculated K_{eq} values for both $^{12}CH_2D_2$ and $^{13}CH_3D$. As a further test, we determined K_{eq}'s using harmonic frequencies calculated to many decimal points of precision directly from published empirical and ab initio force fields [*Jones and McDowell*, 1959—on which the *Bottinga*, 1969 calculation are based; *Gray et al.*, 1979; *Lee et al.*, 1995] and compared these with K_{eq}'s based on tabulated, rounded frequencies from the same studies (Table 1). Discrepancies of up to 0.7‰ are apparent. The 1000ln(K_{eq}) values for $^{12}CH_2D_2$ based on unrounded frequencies (including our ab initio model) span a reasonably narrow range (19.2–19.7) at 300 K, whereas 1000ln(K_{eq}) values based on rounded, tabulated frequencies are more scattered (19.1–20.5).

For the sink reactions, test calculations suggest that the choice of basis sets has little effect on predicted KIEs, as long as the basis set is sufficiently large (i.e., triple-zeta or larger). The choice of model chemistry (i.e., MP2 versus hybrid density functional theory) is more significant. Figures S1 to S4 in the supporting information present these tests. For the reaction with Cl•, the MP2/6-311++G(2d,2p) molecular structures for reactants and products are no more than 0.007 Å different from experimental values [*Boone et al.*, 2001]. For comparison, results of higher-accuracy quadratic configuration interaction with singles and doubles (QCISD) electronic structure models differ from experiment by no more than 0.004 Å [*Boone et al.*, 2001]. KIE results from MP2 model agree well with the models based on the M06 functional [*Zhao and Truhlar*, 2008], which was designed to do well predicting transition state structures and energies. Agreement with B3LYP models [*Becke*, 1993] is poorer. B3LYP is known to perform rather poorly in the prediction of transition states [*Zhao and Truhlar*, 2008]. The most notable difference in the geometry of the transition state structure obtained by MP2 versus B3LYP is in the length of the reacting C---H bond. In the reaction with •OH, the C---H bond oriented toward •OH is 0.034 Å longer with B3LYP models than with MP2 models. Most critically, the imaginary frequency corresponding to the reaction coordinate is $>$700 cm^{-1} higher for MP2 models with H in the reactive C--H bond, and $>$500 cm^{-1} higher with D in the reactive bond. These tests indicate that the MP2 method is well suited for theoretical estimates of KIEs and equilibrium partitioning; in contrast, the B3LYP method may introduce significant additional uncertainty. Therefore, all the reported KIE values in our work are determined using MP2 in combination with the cc-pVTZ basis sets (MP2/cc-pVTZ).

We find systematic differences between theoretical and measured KIE values for singly substituted isotopologues, as has been previously noted [*Gupta et al.*, 1997]. The differences are most noticeable for the Cl• reaction. *Gupta et al.* [1997] reported a 32‰ difference at 300 K between the measured and theoretical $^{13}C/^{12}C$ KIE in the Cl• reaction and a 5‰ difference in the reaction with •OH. The greater isotope sensitivity and

Table 4. Calculated KIEs Compared With Previous Experimental Determinations

	KIE (kCH_4/ki)	Present Study	Calculated Values	Experimental Values
OH	$^{13}CH_4$	1.0063	1.0030 to 1.0094[c]	1.0039 to 1.0059[a,b]
	$^{12}CH_3D$	1.32	1.26 to 1.40[a,c]	1.25[c],1.30[a]
	$^{13}CH_3D$	1.33	1.35[c]	1.34[c]
	$^{12}CH_2D_2$	1.92		1.81[d]
Cl	$^{13}CH_4$	1.028	1.021 to 1.066[e]	1.058[e]
	$^{12}CH_3D$	1.41	1.43 to 1.51[e]	1.46[e]
	$^{13}CH_3D$	1.46	1.48[f]	1.60[f]
	$^{12}CH_2D_2$	2.20	2.16 to 2.93[e]	1.40 to 2.43[g]

[a] *Gola et al.* [2005].
[b] *Cantrell et al.* [1990].
[c] *Joelsson et al.* [2016].
[d] *Gierczak et al.* [1997].
[e] *Feilberg et al.* [2005].
[f] *Joelsson et al.* [2014].
[g] *Sauer et al.* [2015].

theory/experiment disagreement in the Cl• reaction may reflect a transition state that is more product-like, with a longer C---H bond length to the reacting hydrogen atom, compared to a more reactant-like transition state with shorter C--H bonds in the •OH reaction. This means that in the case of Cl•, the reaction coordinate approximates a vibration of a fairly rigid H_3C group against the forming HCl molecule, with significant motion of the carbon atom, whereas the •OH reaction coordinate is mainly translation of the reacting hydrogen atom, with little motion of the carbon atom and thus little carbon isotope sensitivity.

Our model results for doubly substituted isotopologues are in a reasonably good agreement with previous measurements and theoretical studies (Table 4), including KIE values for $^{13}CH_3D$ reactions with •OH and Cl• measured and calculated by *Joelsson et al.* [2016, 2014] (experimental values of 1.34 ± 0.03 and 1.60 ± 0.04 and theoretical values of 1.35 and 1.48 versus our values of 1.33 and 1.46 at 298 K, respectively). The Joelsson et al. measurements used Fourier transform infrared (FTIR) spectroscopy, and the authors suggest that uncertainties stemming from spectral analysis were an important source of uncertainty in their measured KIEs. However, the ultimate cause of the difference between measured and theoretical isotope effects in the reaction with Cl• does not appear to be definitively known [e.g., *Joelsson et al.*, 2014]. The KIE for $^{12}CH_2D_2$, in reactions with •OH and Cl• have also been measured at room temperature in several previous studies. The measured value for the •OH reaction is 1.81 ± 0.28 [*Gierczak et al.*, 1997]. For Cl•, measured values are 2.17 ± 0.2, 2.45 ± 0.05, 2.27 ± 0.27, 1.4 ± 0.2, and 2.19 ± 0.02, respectively, by *Sauer et al.* [2015], *Feilberg et al.* [2005], *Boone et al.* [2001], *Matsumi et al.* [1997], and *Wallington and Hurley* [1992]. The measurement by *Matsumi et al.* [1997] based on an absolute rate determination is in poor agreement with the other studies using relative rate techniques. Impurity in the chemicals and the occurrence of secondary reactions in experimental apparatus could be responsible for some of the scatter in measured KIEs [*Boone et al.*, 2001; *Sauer et al.*, 2015]; however, there is no definite explanation for these differences. Our calculated values for •OH and Cl• are 1.92 and 2.20, respectively, within the range of experimental determinations. In addition, *Feilberg et al.* [2005] list theoretically determined KIE values for $^{12}CH_2D_2$ reacting with Cl• as 2.16, 2.24, 2.40 [*Boone et al.*, 2001], and 2.93 [*Corchado et al.*, 2000]. The lowest theoretical KIE, 2.16, was calculated without considering tunneling effects, however, which are important for this reaction [*Boone et al.*, 2001]. The largest value, 2.93, was determined using a fundamentally different theoretical description of reaction kinetics than transition state theory, which may partly explain the discrepancy relative to the other model results [*Corchado et al.*, 2000]. *Corchado et al.* [2000] acknowledge that their method could result in overestimation of calculated KIE values compared to other experimental and theoretical values, especially at low temperatures. The much smaller difference between the remaining two theoretical results (2.24 versus 2.40) reflects the application of two different tunneling correction factors (Eckhart versus Wigner) [*Boone et al.*, 2001] and may give a reasonable estimate of the intrinsic theoretical uncertainty associated with the use of simplified tunneling corrections for the methane sink reactions. Overall, as seen in Table 4 there is a significant uncertainty and scatter in both measured and theoretically determined KIEs. Even though our theoretical values lie well within the range of previous studies that observation is difficult to convert to a meaningful

confidence interval. However, this uncertainty does not appear to be large enough to qualitatively affect model estimates of the impact that sink reactions on methane isotopologue species in the atmosphere, as we will show below. Our calculated absolute rate constants are also in reasonable agreement with previous published measured and theoretical values by other groups [*Lasaga and Gibbs*, 1991; *Tanaka et al*., 1996]. For example, the *Sander* [2006] experimental rate constant value for CH_4 reacting with •OH at 298 K is 6.3×10^{-15}, whereas our ab initio value is 9.8×10^{-15}. It is perhaps worth mentioning here that *Sauer et al*. [2015] used measured KIEs to make vertical profiles for deuterated methane isotopologues in reaction with Cl•, an exercise bearing some similarity to the atmospheric model we will present in the proceeding sections.

3.2. Steady State Model of Air

Estimated abundances of singly and doubly substituted isotopologues, including $\delta^{13}CH_3D$, $\delta^{12}CH_2D_2$, $\Delta^{13}CH_3D$, and $\Delta^{12}CH_2D_2$, in methane sources to air are shown in Table 3 and in Figures 3 and 4. Using the disequilibrium microbial source budget (DM), $\delta^{13}CH_3D$ and $\delta^{12}CH_2D_2$ for the total atmospheric sources are predicted to be −330‰ and −493‰ (Figure 3) and $\Delta^{13}CH_3D$, and $\Delta^{12}CH_2D_2$ are predicted to be +4.1‰ and +11.8‰, respectively (Figure 4). Both mass-18 isotopologues are enriched relative to the stochastic distribution, mainly due to equilibrium clumping in abiogenic sources, with a small additional enrichment due to mixing. In contrast, $\Delta^{13}CH_3D$ and $\Delta^{12}CH_2D_2$ values for sources using the pseudo-equilibrium microbial assumption (pEM) are +4.8‰ and +21.7‰, respectively. Finally, $\Delta^{12}CH_2D_2$ is +26.6‰ using the predicted values by *Stolper et al*. [2015] (SMC-15). Figure 5 presents a comparison of the effects of the various assumptions for the biogenic methane composition.

A source mixing effect slightly increases $\Delta^{13}CH_3D$ because D/H and $^{13}C/^{12}C$ are positively correlated in the major methane source components ($R^2 \approx 0.37$ for all the sources, weighted equally, and $R^2 \approx 0.60$ for the eight largest source components), and simple mixtures along a positively correlated D/H and $^{13}C/^{12}C$ gradient will have higher $\Delta^{13}CH_3D$ than the weighted average of the end-members, in much the same way that $\Delta^{47}CO_2$ is higher in mixtures between high-$\delta^{18}O$, high-$\delta^{13}C$ and low-$\delta^{18}O$, and low-$\delta^{13}C$ end-members [*Eiler and Schauble*, 2004]. The $\Delta^{12}CH_2D_2$ is similarly expected to increase when sources of varying D/H mix, as shown in the laboratory [*Young et al*., 2016]. The total source composition is thus not at the precise position one would expect from taking a simple weighted average of Δ values in Figure 4.

Having developed an estimate of the source composition, it is interesting to consider the effects of the two major sink reactions on a closed reservoir with an initial composition set equal to the net atmospheric source, as an example of closed-system evolution. We calculated a Rayleigh distillation model at an assumed reaction temperature of −20°C, i.e., ($R = R^0 f^{\alpha-1}$) where f is the fraction remaining of atmospheric methane in reactions with •OH and Cl• (Figures 6 and 7) using the standard relation $\delta^i = \left(\frac{^iR_f}{^iR_{f=1}} - 1\right)(1000‰)$. As the reaction proceeds, δ values increase and Δ values decrease for both mass-18 isotopologues in the remaining methane. This signature is much more pronounced for $^{12}CH_2D_2$ (Figure 7). For example, in reaction with •OH, when f = 0.5 (50% of methane remaining) $\Delta^{13}CH_3D$ has changed from +4.1‰ to +3.3‰, but ΔCH_2D_2 changed from +11.8‰ to +4.2‰. Analogous shifts in the Cl• reaction at f = 0.5 are −2.1‰ and −22.4‰, respectively. The much larger effects on $\Delta^{12}CH_2D_2$ suggest that $^{12}CH_2D_2$ measurements are likely to be particularly well suited for investigating the overall atmospheric methane budget, especially secular changes in source and sink fluxes, while $^{13}CH_3D$ may give a more focused picture of source components.

In contrast to the closed-system Rayleigh model, a steady state model for atmospheric CH_4 with the DM source assumption predicts $\Delta^{13}CH_3D$ and $\Delta^{12}CH_2D_2$ values of +4.5‰ and +113.5‰, respectively, with a large enrichment of $^{12}CH_2D_2$ above the stochastic reference. The $\delta^{13}CH_3D$ and $\delta^{12}CH_2D_2$ values are −98.7‰ and −11.7‰, respectively, in this model. Steady state values for $\delta^{13}C$ and δD are ~ −48‰ and ~ −58‰, which are reasonably close to the composition of the modern troposphere (−47‰ and −86‰ [*Quay et al*., 1999]) (Figure 8). The alternative pseudo-equilibrium microbial (pEM) source composition yields steady state air values for $\Delta^{13}CH_3D$ of ~ +5‰ and $\Delta^{12}CH_2D_2$ of ~ +124‰, while $\Delta^{12}CH_2D_2$ (steady state) is ~ +130‰ using the *Stolper et al*. [2015] source composition (SCM-15) (Figure 9). Overall,

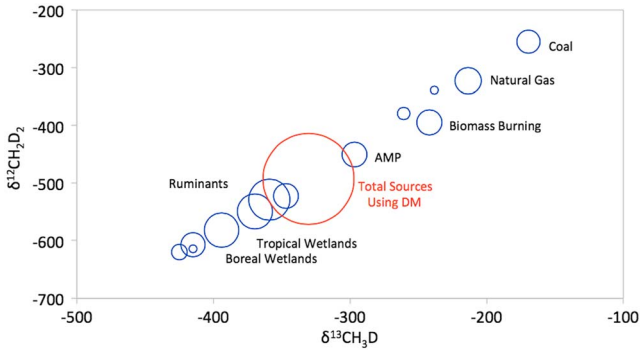

Figure 3. Estimated fluxes, $\delta^{12}CH_2D_2$ and $\delta^{13}CH_3D$ for methane sources to the atmosphere, based on the disequilibrium model (DM). The area of each circle is scaled in proportion to the flux it represents.

steady state models with various source assumptions predict that the main sink reactions in the atmosphere generate a distinct signature of higher $\Delta^{12}CH_2D_2$ relative to the source composition, also increasing $\delta^{13}CH_3D$ and $\delta^{12}CH_2D_2$. These predictions illustrate the importance of the sink reactions in controlling the relative abundance of $^{12}CH_2D_2$ in atmosphere, as well as the distinct signature of an open system with sinks and sources, relative to either process acting in isolation. They also suggest that $\Delta^{13}CH_3D$ will mainly be sensitive to source compositions, in agreement with another recent theoretical and experimental study of $\Delta^{13}CH_3D$, which predicts only an ~0.3‰ impact of the sink reactions on tropospheric methane [*Whitehill et al.*, 2017].

As mentioned earlier, it is well known that Δ values can show behavior distinct from δ as the result of mixing, diffusion, or kinetic isotope effects [*Eiler and Schauble*, 2004; *Eiler*, 2007]. This occurs because the stochastic reference frame changes with the isotopic composition of the gas. The $\Delta^{12}CH_2D_2$ in our steady state model shows analogous behavior, which might be rationalized as an ongoing, mixing-like process between fresh source gas with low D/H and fractionated sink residue with roughly 210‰ higher D/H.

3.3. Isotopologue Signatures of Unbalanced Sources and/or Sinks

The recent rise in atmospheric methane could be the result of an increase in emission rate, a decrease in sink activity (via reduction in the concentration of the hydroxyl radical), or a combination of both [*Rigby et al.*, 2008; *Bousquet et al.*, 2006]. The roles of the individual emission sources in affecting the recent change of global atmospheric methane are uncertain. Therefore, in our dynamic model, we examined a number of different possibilities. After imposing changes in sources and/or sinks we monitored the evolution $\delta^{13}C$ ($\delta^{13}CH_4$), δD ($\delta^{12}CH_3D$), $\Delta^{13}CH_3D$, and $\Delta^{12}CH_2D_2$ of methane in the atmospheric air over time (Figures 10–13).

3.3.1. Instantaneous Doubling of Source Components

For the first set of tests we assumed no change in the sink reaction rates and changed global emission sources to force the model out of balance. In each case, an impulse (sudden change in rate) was imposed by doubling the flux of one of the major sources (e.g., Figure 10). In the case of doubling wetland rates of methane emission, the initial $\Delta^{12}CH_2D_2$ response is a transient starting with a sudden increase to 3.0‰ above the steady state value of 113.5‰ lasting 2 years, followed by a 7.8‰ decrease over an ~30 year period and then a gradual 8.0‰ increase, settling to a new steady state value of 116.7‰ after ~150 years. Instantaneous doubling of wetland output therefore has a net effect of approximately 3‰ in $\Delta^{12}CH_2D_2$ over a period of a century and a half.

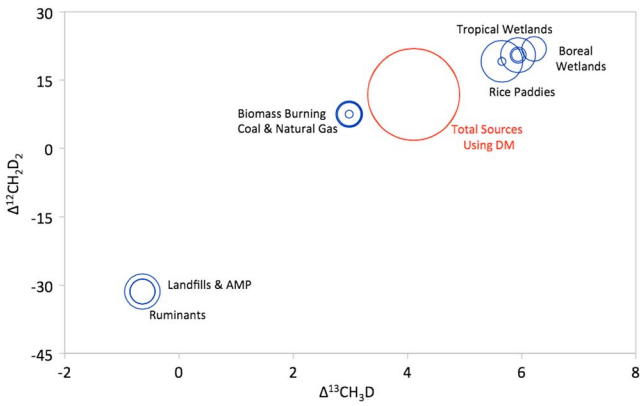

Figure 4. Estimated $\Delta^{12}CH_2D_2$ and $\Delta^{13}CH_3D$ in methane sources to air, based on the disequilibrium model (DM). The area of each circle is scaled in proportion to the flux it represents.

Doubling both biomass burning and coal emission yields results similar to that for wetlands. The doubling of

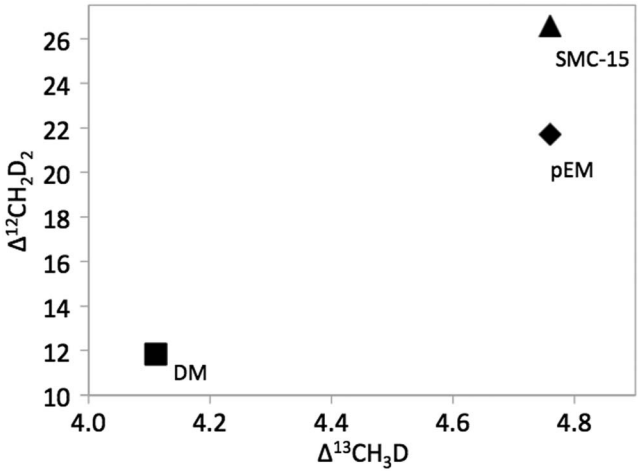

Figure 5. A comparison of the effects of different source model assumptions for isotopologue abundances in biogenic methane (disequilibrium model: DM, pseudo-equilibrium model: pEM, *Stolper et al.* [2015] model: SMC-15) on the calculated $\Delta^{13}CH_3D$ and $\Delta^{12}CH_2D_2$ of the total atmospheric methane source.

these sources causes an initial 11.0‰ decrease over approximately 25 years followed by an 13.4‰ increase to the new steady state value of 116.0‰ after roughly 120 years. For the case of doubling rice paddies, there is a sudden initial increase of 0.7‰ lasting for 2 years to a maximum value of 114.2‰, then a decrease of 9.2‰ to a minimum of 105‰ and finally attainment of a new steady state of 115.0‰ over a total period of around 120 years (Figure 10b).

The effects of emission impulses on $\Delta^{13}CH_3D$ are much smaller (Figures 10c). For example, doubling wetland emission causes an initial 0.3‰ increase from the steady state value of 4.5‰, then a 0.05‰ decrease lasting for ~20 years and again a 0.1‰ increase to a new steady state of 4.9‰, a net increase of 0.4‰. In the case of doubling methane production from rice paddies, an initial increase in $\Delta^{13}CH_3D$ of 0.3‰ lasting for 5 years is followed by a 0.1‰ decrease and then a final 0.1‰ increase to reach the new steady state value of ~4.8‰, or a net increase of 0.3‰. Doubling biomass and coal burning produces a 12 year period of decrease of 0.3‰ followed by a 0.5‰ increase, reaching the new steady state value of 4.7‰ after ~70 years.

Considering these perturbation scenarios in concert, it appears that the KIEs associated with sink reactions lead to distinct lifetimes for different methane isotopologues and large contrasts between the isotopic compositions of the source flux and the atmosphere. The effects combine to cause rather complex annual to decadal patterns of variation in isotopologue abundance ratios in nonsteady state box models. The complexity reflects the residence times of $^{12}CH_4$, $^{13}CH_4$, $^{12}CH_3D$, $^{13}CH_3D$, and $^{12}CH_2D_2$ in the atmosphere with respect to reaction with •OH and Cl• of 10.9, 11.0, 14.6, 14.7, and 21.5 years, respectively. Broadly speaking, increases in source flux lead to a temporary (<10 years) decrease in the D/H of atmospheric methane and variation in the $^{12}CH_2D_2$ excess as the reservoir mixes toward the source composition, but the reservoir moves toward a new steady state on longer timescales that roughly restores the original source/atmosphere offset in D/H (with a characteristic timescale of ~15 years) and $^{12}CH_2D_2$ excess (~22 years). Intermediate high-frequency variations may come from the distinct timescales for the evolution of the normal, singly, and doubly substituted isotopologues. We

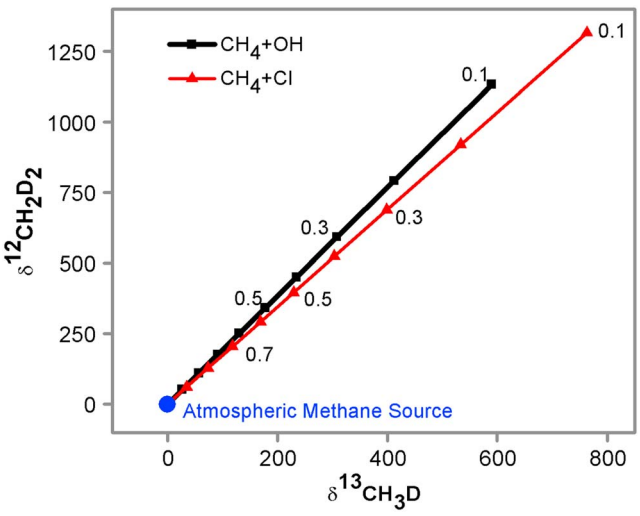

Figure 6. Estimated $\delta^{13}CH_3D$ and $\delta^{12}CH_2D_2$ in the residual gas in a Rayleigh distillation model. The initial reservoir is assumed to have the atmospheric source composition predicted by the disequilibrium model (DM). The −20°C (253 K) KIEs for the •OH (black thick line) and Cl• (red thin line) sink reactions are used. The tickmarks and labels indicate the fraction of gas remaining.

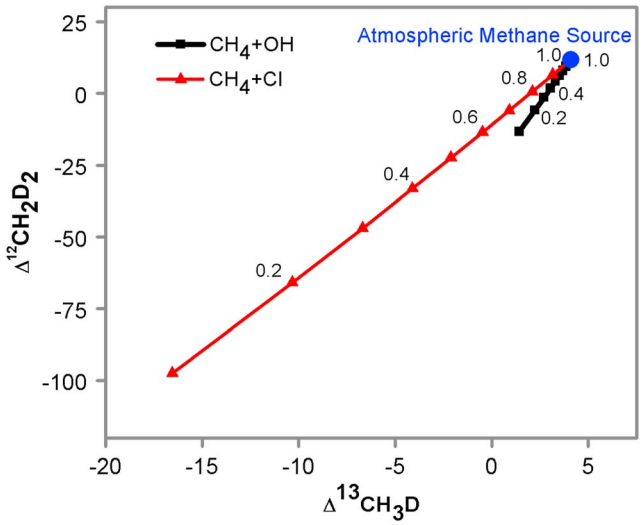

Figure 7. Estimated $\Delta^{13}CH_3D$ and $\Delta^{12}CH_2D_2$ in the residual gas in a Rayleigh distillation model. The initial reservoir is assumed to have the atmospheric source composition predicted by the disequilibrium model (DM). The −20°C (253 K) KIEs for the •OH (black thick line) and Cl• (red thin line) sink reactions are used. The tickmarks and labels indicate the fraction of gas remaining.

also observe, for both $\Delta^{12}CH_2D_2$ and $\Delta^{13}CH_3D$, that short- and (especially) long-term responses to variations in individual source component fluxes scale to some extent with their effects on the net $\Delta^{12}CH_2D_2$ and $\Delta^{13}CH_3D$ of the total source. However, it should be emphasized that changes in the total source flux also have short-term (years to decades) effects even in the absence of any change in the isotopic composition of the total source.

3.3.2. Change in •OH Concentration

In order to examine the effects of changing sink rates we imposed an instantaneous change in the concentration of •OH in the atmosphere (Figures 11). The atmospheric methane budget is very sensitive to •OH concentration changes. *Dlugokencky et al.* [1996] suggested that in 1991/1992 the reduction of •OH as the result of the Mount Pinatubo volcanic eruption could be the reason behind the rise of atmospheric methane in that year. •OH concentrations in the atmosphere could also be effected by changes in the levels of atmospheric carbon monoxide (CO), the main •OH sink [*Rigby et al.*, 2008]. Reported year-to-year changes in •OH concentration vary from 2% [*Montzka et al.*, 2011] to 25% with a reported mean interannual variability of ~7 to 9% [*Bousquet et al.*, 2005; *Prinn et al.*, 2005]. We therefore examined changes in •OH concentrations of ±5% as a plausible short-term step. A 5% increase in [•OH] results in an initial $\Delta^{12}CH_2D_2$ transient consisting of an increase of 3‰ to a value of 116.5‰. The excursion requires over a decade to reach its maximum amplitude. This is much longer than the timescale of interest for small interannual variations. In contrast, the induced variation in the first year after the perturbation is less than 1‰. In the model scenario, $\Delta^{12}CH_2D_2$ reverts gradually back to a steady state of 113.6‰ over the next century or two (Figure 11b, black line), ending up very close to the initial steady state composition. For $\Delta^{13}CH_3D$ the same change in [•OH] causes a sudden but much more modest decrease of less than 0.1‰ from the initial +4.5‰ lasting ~3 years followed by a 0.05‰ increase over an ~30 year period and then a 0.03‰ decrease to a new steady state value of 4.6‰ over the next century (Figure 11c, black line), reflecting the slightly changed balance of sink reactions with Cl• versus •OH. A 5% decrease in [•OH] results in nearly the opposite response to a 5% increase (Figure 11b, dashed red line, and Figure 11c. dashed red line), and a 10% decrease or increase results in almost exactly twice the amplitude of variation with similar timescales, consistent with the scaling observed for source variations.

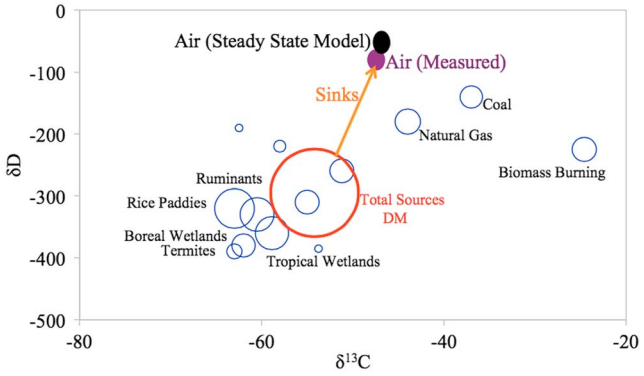

Figure 8. Singly substituted isotopologue signatures (δD and $\delta^{13}C$) of methane sources to air in the disequilibrium model (DM) compared to the steady state composition using calculated KIEs for sink reactions with •OH and Cl•. The measured atmospheric composition is also shown [*Quay et al.*, 1999].

3.3.3. Exponentially Increase in Emission

Changes in atmospheric methane concentrations may also result from

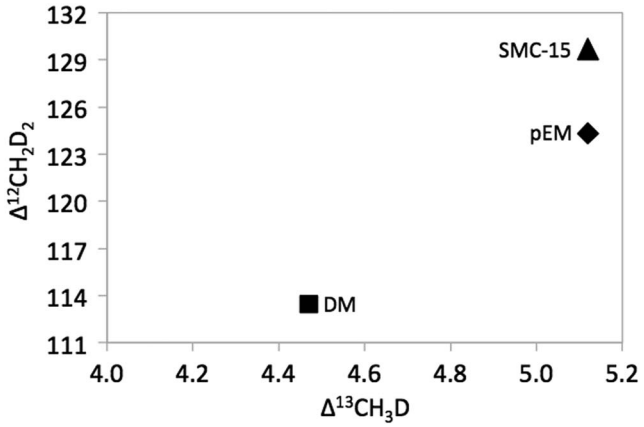

Figure 9. Doubly substituted isotopologue signatures ($\Delta^{13}CH_3D$ and $\Delta^{12}CH_2D_2$) in air at steady state composition using the disquilibrium model (DM), pseudo-equilibrium model (pEM), and *Stolper et al.* [2015] measurements and model (SCM-15) source compositions, and calculated KIEs for reaction with •OH (96.6%) at 262 K and Cl• (3.4%) at 273.

more gradual changes in sources. For instance, according to *Bousquet et al.* [2006], variations in wetland emissions were the main control of interannual variability in total source emissions (±12 Tg of CH_4/yr) during the 20 year period between 1984 and 2004. Such wetland-dominated variability could explain 70% of global emission anomalies in this period. In order to approximate such a change we investigated the effects of exponentially changing source terms, extending the exponential increase out to a duration of 200 years to see how long-term, modest rates of increase compare to faster, shorter-lived scenarios (Figure 12). We examined exponential growth rates of 1%/yr in the emission from all sources and a 5%/yr exponential increase in wetland source emissions with no change in other sources.

For the first case where all sources increase, $\Delta^{12}CH_2D_2$ declines from 113.5‰ to 85.0‰ over a time interval of 150 years (Figure 12c, black line) during which overall emissions increased by more than 600%. The $\Delta^{13}CH_3D$ increases from 4.5‰ to 4.6‰ and then decreases to 4.2‰ in this scenario (Figure 12d, black line). In the case of a more rapidly increasing wetland source we first see an increase in $\Delta^{12}CH_2D_2$ of 2.0‰ from the steady state value of 113.5‰, and then a protracted reduction to a new steady state of ~49.0‰ over the next ~160 years (Figure 12c, dashed red line). In this scenario, $\Delta^{13}CH_3D$ increases from the steady state value of 4.5‰ to a new steady state of 5.8‰ over this same time interval (Figure 12d, dashed red line). Such a large exponential increase in wetland emission over 200 years is obviously unrealistic, but it does illustrate the asymptotic effects of long-term trends in source budgets.

In the scenario with a 5%/yr exponential increase in wetland source emissions, the total wetland emissions have doubled after 14 years, and at this stage the perturbation from steady state $\Delta^{12}CH_2D_2$ and $\Delta^{13}CH_3D$ are rather similar to those found roughly 2–3 years after an instantaneous doubling wetland emissions.

3.3.4. Seasonal Cycling in Wetland Emission

Finally, we developed a model with seasonal variations in wetland emission sources, simulating changes in surface temperature, precipitation, and other seasonal parameters, but also to serve more broadly as an analogue scenario for various proposed and observed intraannual and short-term interannual variations in other source and sink components of the overall budget. We left the total integrated annual wetland emission unchanged, assuming an oscillation with a period of 1 year, ranging from no wetland emissions in month zero to twice the average annual wetland flux rate in month six. We observe in the model that variations in the atmospheric reservoir caused by rapid seasonal oscillations are strongly damped by the much longer residence time of methane, resulting in only a small seasonal variation in $\Delta^{12}CH_2D_2$ (Figure 13b) of order ~0.5‰. Similarly, $\Delta^{13}CH_3D$ varies by less than 0.1‰ (Figure 13c) in this scenario. Overall it seems that seasonal cycling of wetland sources will only induce minor isotopic variations in the atmospheric reservoir as a whole. This is true not only for clumping signals but also for the bulk δD, which varies by only 1.9‰; $\delta^{13}C$ varies by only 0.1‰ (Figures 13d and 13e). By comparison, the amplitude of the seasonal cycle in $\delta^{13}C$ observed by *Quay et al.* [1999] ranges from ~0.1‰ to 0.4‰, depending on latitude.

The $\Delta^{12}CH_2D_2$ and $\Delta^{13}CH_3D$ seem to have the potential to reveal more information about the global atmosphere CH_4 budget, particularly on multiyear timescales. However, it should be noted that the potential for significant short-term perturbation signatures has not been examined at smaller spatial scales (e.g., versus latitude or altitude) where source/sink balances may vary more dramatically, and short-term isotopic and isotopologue abundance variations may be larger.

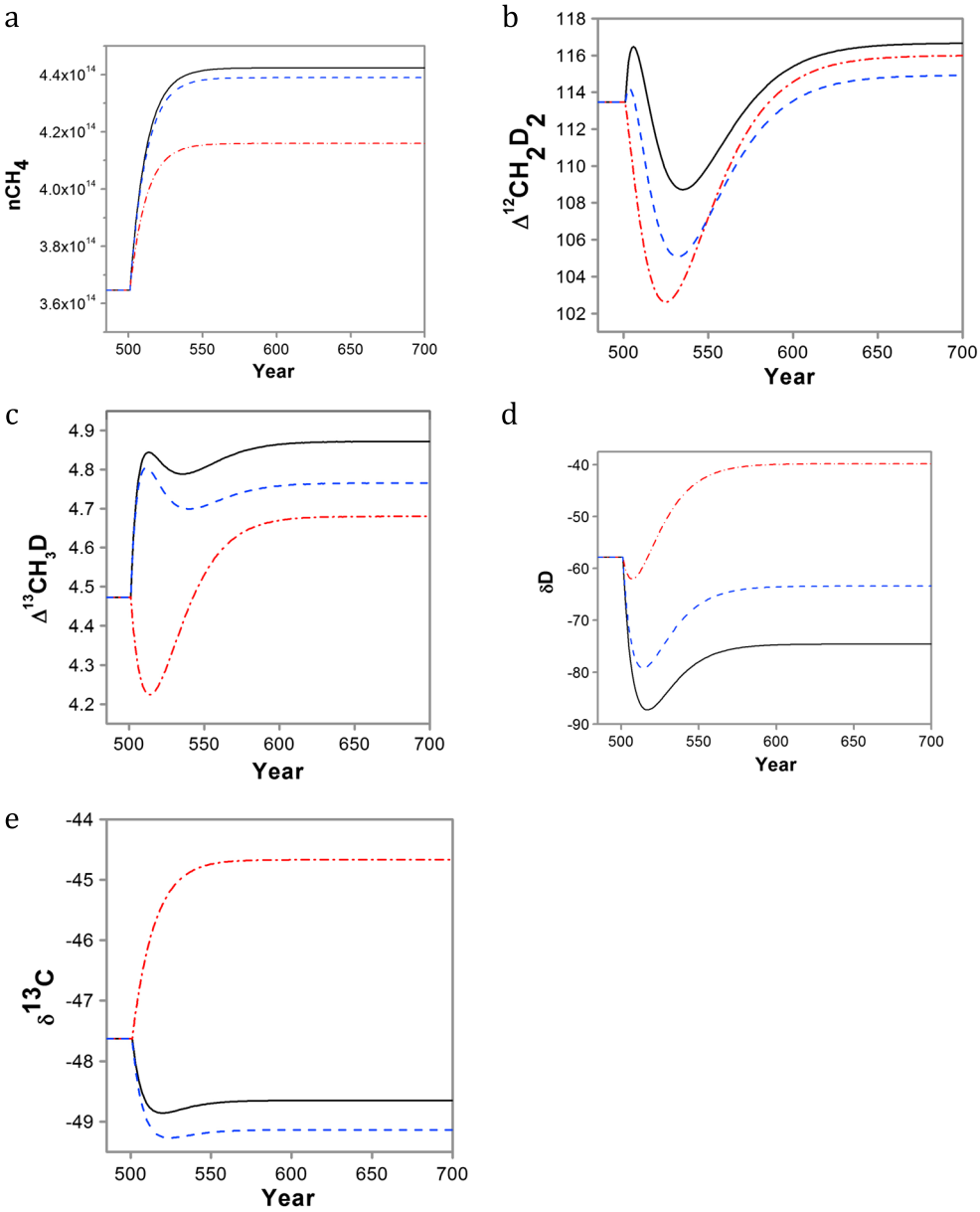

Figure 10. Dynamic box model results for a sudden, permanent doubling of wetland emissions (black line), rice paddy emissions (blue dashed line), and biomass and fossil fuel emissions (red dashed-dot line) to the atmosphere, starting from steady state: (a) number of moles of CH_4 in the atmosphere, (b) $\Delta^{12}CH_2D_2$ in air, (c) $\Delta^{13}CH_3D$ in air, (d) δD in air, and (e) $\delta^{13}C$ in air.

3.4. Sensitivity Testing

3.4.1. Alternative Source Budgets

Global atmospheric methane budgets have previously been estimated using two basic approaches. So far, we have followed a bottom-up estimated budget, as reported by *Whiticar and Schaefer* [2007] that is consistent with a total source flux of 540 Tg/yr. Coincidentally, this total flux value is the same as the *IPCC* [2013] reported value, even though that estimate is based on a top-down approach. The contributions from individual source components do differ between the two compilations.

In order to get a more extreme test of the sensitivity of the box model results to the source compositions, we altered our initial source budget to match the IPCC alternative "bottom-up" budget, which yields a total source flux of 678 Tg/yr, without changing the isotope and isotopologue compositions of each source component. Despite the change in overall flux, the altered budget yields a change of

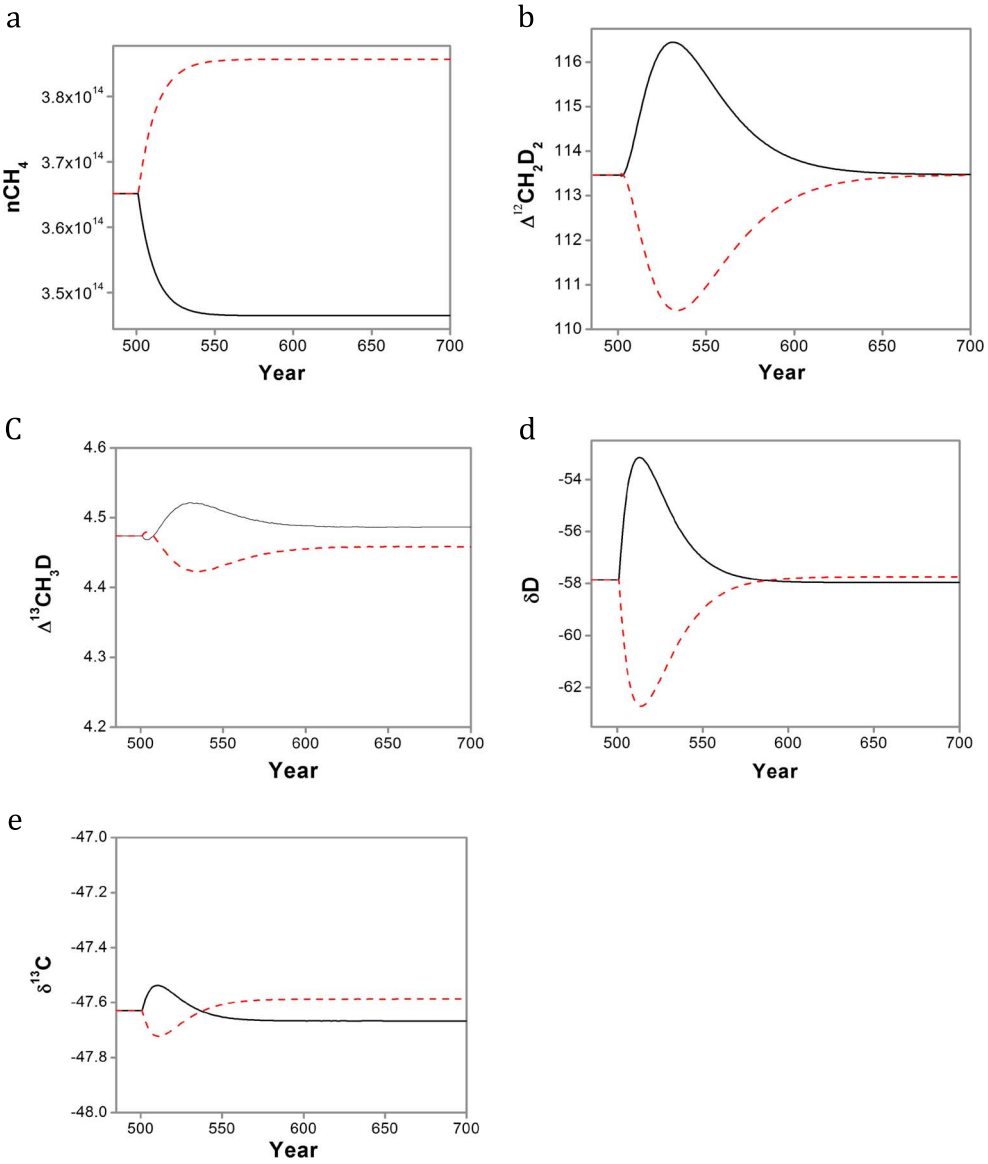

Figure 11. Dynamic box model results for a sudden, permanent 5% increase (black line), and 5% decrease (dashed red line) in atmospheric OH radical concentration, starting from steady state: (a) number of moles of CH_4 in the atmosphere, (b) $\Delta^{12}CH_2D_2$ in air, (c) $\Delta^{13}CH_3D$ in air, (d) δD in air, and (e) $\delta^{13}C$ in air.

only +0.1‰ in the predicted $\Delta^{13}CH_3D$ and +3.0‰ in $\Delta^{12}CH_2D_2$ for the total estimated source composition and similar changes in the steady state atmospheric composition. Applying the steady state model using these source flux estimates, $\Delta^{13}CH_3D$ in air will be +4.6‰ and $\Delta^{12}CH_2D_2$ will be +116.8‰ (Figure 14).

Similar to the calculations described in section 3.3.1., for example, doubling emission from wetland sources (holding all source component isotopic compositions fixed) caused source $\Delta^{13}CH_3D$, and $\Delta^{12}CH_2D_2$ signatures to increase by 0.4‰ and 3‰ to values of +4.5‰ and +14.8‰, respectively. Doubling the flux from rice paddies led to a change of +0.3‰ in $\Delta^{13}CH_3D$ and +1.4‰ in $\Delta^{12}CH_2D_2$. Doubling the emission of coal and biomass burning leads to changes of +0.2‰ and +2.30‰ in $\Delta^{13}CH_3D$ and $\Delta^{12}CH_2D_2$, respectively (Figure 14). More details are in the supporting information. Overall these tests suggest that uncertainties in the rate of emissions from various major sources will likely contribute uncertainties of ~1‰ and several ‰ to the net source $\Delta^{13}CH_3D$ and $\Delta^{12}CH_2D_2$, respectively.

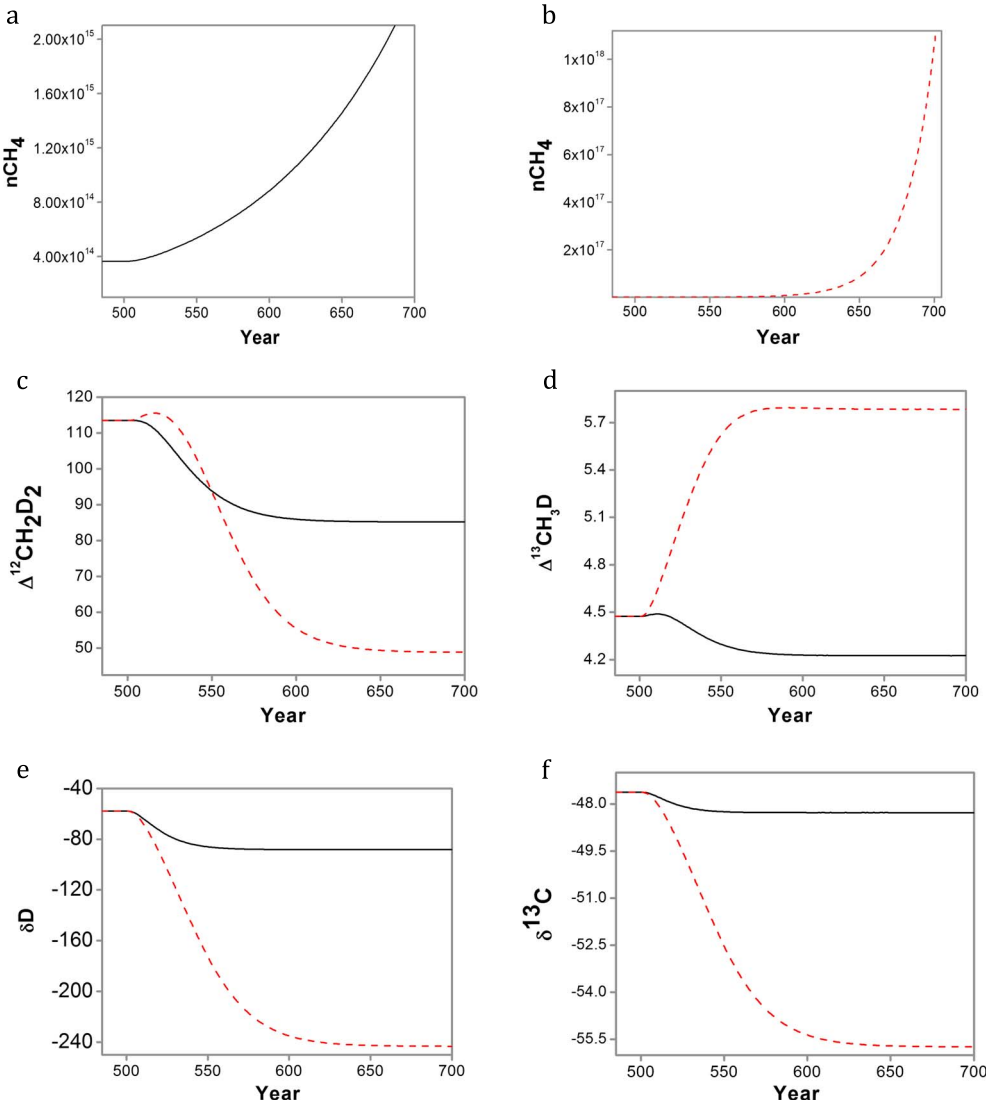

Figure 12. Dynamic box model results for exponentially increasing total CH_4 emissions (+1%/yr) (black line), and wetland emissions (+5%/yr) (dashed red line), starting from steady state: (a and b) number of moles of CH_4 in the atmosphere, (c) $\Delta^{12}CH_2D_2$ in air, (d) $\Delta^{13}CH_3D$ in air, (e) δD in air, and (f) $\delta^{13}C$ in air.

3.4.2. KIEs and Sinks

As an initial test of the sensitivity of our atmospheric budgets to uncertainties or changes in kinetic isotope effects in the sink reactions, we constructed a simple heuristic KIE model in which we assumed that D cannot be abstracted from methane into the water vapor or HCl product in the reaction between CH_4 and •OH or Cl•; i.e., we assume that $k_{CH3D} = 3/4k_{CH4}$ and $k_{CH2D2} = 1/2k_{CH4}$, consistent with the rule of the geometric mean [*Bigeleisen*, 1955], and for simplicity further assumed that carbon isotope effects are absent in both sink reactions. The resulting atmospheric steady state compositions are qualitatively similar to results using ab initio KIEs for all three deuterated isotopologues studied ($^{12}CH_3D$, $^{13}CH_3D$, and $^{12}CH_2D_2$). For $\Delta^{12}CH_2D_2$, the resulting steady state atmospheric value is still notably enriched relative to the source composition at +138‰, which is about 24‰ higher than the steady state composition reached results using ab initio KIEs. At steady state the atmospheric $\Delta^{13}CH_3D$ retains the source value in the heuristic model, because it is assumed that there in no ^{13}C-related KIE.

As a second test, we used experimentally determined KIEs of sink reactions [*Gola et al.*, 2005; *Joelsson et al.*, 2016; *Gierczak et al.*, 1997; *Feilberg et al.*, 2005; *Joelsson et al.*, 2014] to determine $\Delta^{13}CH_3D$ and

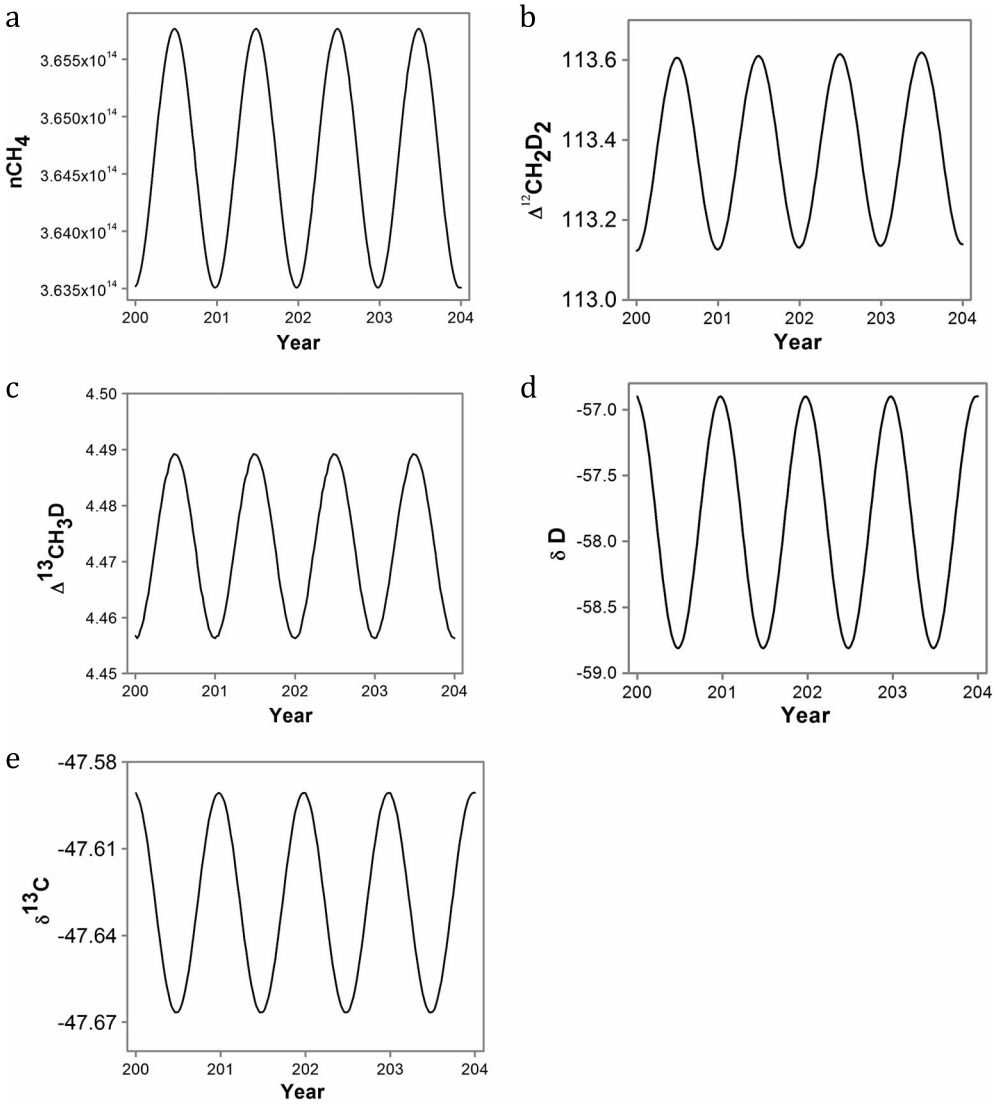

Figure 13. Dynamic box model results for seasonally variable wetland emissions (from zero in month zero to the twice the average annual wetland flux value in month six), starting from steady state: (a) number of moles of CH_4 in the atmosphere, (b) $\Delta^{12}CH_2D_2$ in air, (c) $\Delta^{13}CH_3D$ in air, (d) δD in air, and (e) $\delta^{13}C$ in air.

$\Delta^{12}CH_2D_2$ of air rather than our ab initio model. The steady state $\Delta^{13}CH_3D$ and $\Delta^{12}CH_2D_2$ values we obtain are +33.80 ± 26.00‰ and +101.20 ± 51.40‰, respectively. These compositions overlap with our model steady state values using ab initio KIEs, albeit with a large range of scatter. In all cases, however, the steady state $\Delta^{12}CH_2D_2$ is strongly enriched by the open system interaction between sources and sinks.

4. Conclusions

For the first time, expected signatures in the abundances of doubly substituted mass-18 methane isotopologues ($^{13}CH_3D$ and $^{12}CH_2D_2$) have been incorporated into a box model for the atmospheric methane budget. $^{13}CH_3D$ and $^{12}CH_2D_2$ show promise as complementary tracers of atmospheric methane sources and sinks under some circumstances, with $^{12}CH_2D_2$ in particular being sensitive to sink reactions. However, in order to make the best use of mass-18 isotopologue measurements in air, it will be important to accurately characterize the major sources and sinks of atmospheric methane in terms of flux, isotopic composition, and isotopologue signatures.

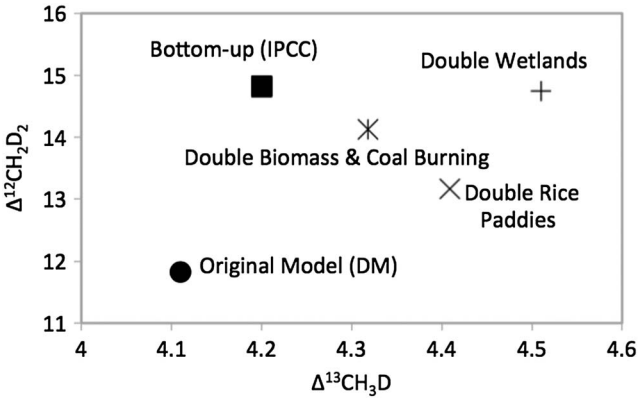

Figure 14. Sensitivity of the total atmospheric source model composition to changes in fluxes from various source components. A comparison between estimated $\Delta^{13}CH_3D$, and $\Delta^{12}CH_2D_2$ values of total atmospheric sources when doubling: wetland sources, biomass, and coal sources, and rice paddies individually along with using bottom-up total source emissions.

We have demonstrated that the reactions of methane with •OH and Cl• generate a distinct signature of higher $\Delta^{12}CH_2D_2$ (by ~102‰ using our ab initio KIEs) relative to the source composition. We predict high $\Delta^{12}CH_2D_2$ values of ~114‰ relative to stochastic in air at approximate steady state, in contrast to $\Delta^{13}CH_3D$ values of ~5‰ that are little different from the estimated source composition. The largest sensitivities in mass-18 isotopologue abundances come from changes in the wetland source term in our model. The effects of changing sink rates due to changing •OH concentrations are more modest but may still be measurable. Although the precision of measurements of $^{13}CH_3D$ is better compared to $^{12}CH_2D_2$ [*Young et al*., 2017], the range of variation in composition is so much larger for $^{12}CH_2D_2$ that the doubly deuterated isotopologue is still likely to be a more sensitive probe for investigating these types of variation in the atmospheric methane budget. Our predictions may be useful for constraining the origin and fate of methane in the atmosphere. The characteristic relationship between $\Delta^{13}CH_3D$ versus $\Delta^{12}CH_2D_2$ may make it possible to back-project from the composition of methane in air to constrain contributions from individual sources and sinks.

Acknowledgments
This study was supported in part by grants from the U.S. National Science Foundation (EAR1530306 and EAR1047668), the American Chemical Society Petroleum Research Fund, and from the Deep Carbon Observatory. All electronic structure calculations in this study are made using the Gaussian09 software package (Gaussian 09: AM6 4 L-G09RevB.01 12 August 2010) on the UCLA Hoffman2 cluster. Supporting data are included in the supporting information. Correspondence and requests for materials and data should be addressed to Mojhgan Haghnegahdar (mojhganh-gh@ucla.edu). Laurence Yeung is thanked for suggestions early on in this project.

References

Alei, M., et al. (1987), Determination of deuterated methanes for use as atmospheric tracers, *Atmos. Environ.*, *21*, 909–915.
Allan, W., H. Struthers, and D. C. Lowe (2007), Methane carbon isotope effects caused by atomic chlorine in the marine boundary layer: Global model results compared with Southern Hemisphere measurements, *J. Geophys. Res.*, *112*, D04306, doi:10.1029/2006JD007369.
Assonov, S. S., and C. A. M. Brenninkmeijer (2003), On the ^{17}O correction for CO_2 mass spectrometric isotopic analysis, *Rapid Commun. Mass Spectrom.*, *17*(10), 1007–1016.
Becke, A. D. (1993), Density-functional thermochemistry. III. The role of exact exchange, *J. Chem. Phys.*, *98*(7), 5648.
Bigeleisen, J. (1955), Statistical mechanics of isotopic systems with small quantum corrections, I. General considerations and the rule of the geometric mean, *J. Chem. Phys.*, *23*(1955), 2264–2267.
Boone, G. D., F. Agyin, D. J. Robichaud, F. Tao, and S. A. Hewitt (2001), Rate constants for the reactions of chlorine atoms with deuterated methanes: Experiment and theory †, *Reactions*, 1456–1464.
Bottinga, Y. (1969), Calculated fractionation factors for carbon and hydrogen isotope exchange in the system, *Geochim. Cosmochim. Acta*, *33*, 49–64, doi:10.1016/0016-7037(69)90092-1.
Bousquet, P., D. a. Hauglustaine, P. Peylin, C. Carouge, and P. Ciais (2005), Two decades of OH variability as inferred by an inversion of atmospheric transport and chemistry of methyl chloroform, *Atmos. Chem. Phys. Discuss.*, *5*(2), 1679–1731.
Bousquet, P., et al. (2006), Contribution of anthropogenic and natural sources to atmospheric methane variability, *Nature*, *443*, 439–443, doi:10.1038/nature05132.
Bousquet, P., et al. (2011), Source attribution of the changes in atmospheric methane for 2006–2008, *Atmos. Chem. Phys.*, *11*, 3689–3700, doi:10.5194/acp-11-3689-2011.
Bréas, O., C. Guillou, F. Reniero, and E. Wada (2001), The global methane cycle: Isotopes and mixing ratios, sources and sinks, *Isot. Environ. Health Stud.*, *37*(4), 257–379, doi:10.1080/10256010108033302.
Cantrell, C. A., R. E. Shetter, A. H. McDaniel, J. G. Calvert, J. A. Davidson, D. C. Lowe, and J. P. Greenberg (1990), Carbon kinetic isotope effect in the oxidation of methane by the hydroxyl radical, *J. Geophys. Res.*, *95*, 22,455–22,462, doi:10.1029/JD095iD13p22455.
Cao, X., and Y. Liu (2012), Theoretical estimation of the equilibrium distribution of clumped isotopes in nature, *Geochim. Cosmochim. Acta*, *77*, 292–303, doi:10.1016/j.gca.2011.11.021.
Cicerone, R. J., and R. S. Oremland (1988), Biochemical aspects of atmospheric methane, *Global Biochem. Cycles*, *2*, 299–327, doi:10.1029/GB002i004p00299.
Corchado, J. C., D. G. Truhlar, and J. Espinosa-García (2000), Potential energy surface, thermal, and state-selected rate coefficients, and kinetic isotope effects for $Cl + CH_4 \rightarrow HCl + CH_3$, *J. Chem. Phys.*, *112*, 9375, doi:10.1063/1.481602.
Dlugokencky, E. J., L. P. Steele, P. M. Lang, and K. A. Masarie (1994), The growth rate and distribution of atmospheric methane, *J. Geophys. Res.*, *99*, 17,021–17,043, doi:10.1029/94JD01245.
Dlugokencky, E. J., E. G. Dutton, P. C. Novelli, and P. P. Tans (1996), Changes in CH_4 and CO growth rates after the eruption of Mt. Pinatubo and their link with changes in tropical tropospheric UV flux, *Geophys. Res. Lett.*, *23*, 2761–2764, doi:10.1029/96GL02638.
Dlugokencky, E. J., E. G. Nisbet, R. Fisher, and D. Lowry (2011), Global atmospheric methane: Budget, changes and dangers, *Philos. Trans. Ser. A Math. Phys. Eng. Sci.*, *369*(1943), 2058–2072, doi:10.1098/rsta.2010.0341.

Douglas, P. M. J., et al. (2016), Diverse origins of Arctic and Subarctic methane point source emissions identified with multiply-substituted isotopologues, *Geochim. Cosmochim. Acta*, *188*, 163–188, doi:10.1016/j.gca.2016.05.031.

Dunning, T. H., Jr. (1989), Gaussian basis sets for use in correlated molecular calculations. I. The atoms boron through neon and hydrogen, *J. Chem. Phys.*, *90*(1989), 1007, doi:10.1063/1.456153.

Eiler, J. M. (2007), "Clumped-isotope" geochemistry—The study of naturally-occurring, multiply-substituted isotopologues, *Earth Planet. Sci. Lett.*, *262*, 309–327, doi:10.1016/j.epsl.2007.08.020.

Eiler, J. M., and E. Schauble (2004), $^{18}O^{13}C^{16}O$ in Earth's atmosphere, *Geochim. Cosmochim. Acta*, *68*(23), 4767–4777, doi:10.1016/j.gca.2004.05.035.

Feilberg, K. L., D. W. T. Griffith, M. S. Johnson, and C. J. Nielsen (2005), The ^{13}C and D kinetic isotope effects in the reaction of CH_4 with Cl, *Int. J. Chem. Kinet.*, *37*(2), 110–118, doi:10.1002/kin.20058.

Fletcher, S. E. M., P. P. Tans, L. M. Bruhwiler, J. B. Miller, and M. Heimann (2004), CH4 sources estimated from atmospheric observations of CH4 and its 13C/12C isotopic ratios : 1.Inverse modeling of source processes, *Global Biogeochem. Cycles*, *18*, GB4004, doi:10.1029/2004GB002223.

Fung, I., J. John, J. Lerner, E. Matfhews, M. Prather, L. P. Steele, and P. J. Fraser (1991), Three-dimensional model synthesis of the global methane cycle, *J. Geophys. Res.*, *96*, 13,033–13,065, doi:10.1029/91JD01247.

Frisch, M. J., et al. (2013), *Gaussian 09: EM64L-G09RevD.01*, Gaussian, Wallingford, Conn.

Gierczak, T., R. K. Talukdar, S. C. Herndon, G. L. Vaghjiani, and A. R. Ravishankara (1997), Rate coefficients for the reactions of hydroxyl radicals with methane and deuterated methanes, *Chem. Eur. J.*, *101*(17), 3125–3134, doi:10.1021/jp963892r.

Gola, A. A., B. D'Anna, K. L. Feilberg, S. R. Sellevåg, L. Bache-Andreassen, and C. J. Nielsen (2005), Kinetic isotope effects in the gas phase reactions of OH and Cl with CH_3Cl, CD_3Cl, and $^{13}CH_3Cl$, *Atmos. Chem. Phys.*, *5*, 2395–2402, doi:10.5194/acp-5-2395-2005.

Gray, D. L., A. G. Robiette, and A. S. Pine (1979), Extended measurement and analysis of the ν3 infrared band of methane, *J. Mol. Spectrosc.*, *77*(3), 440–456, doi:10.1016/0022-2852(79)90183-8.

Gupta, M. L., M. P. Mcgrath, R. J. Cicerone, F. S. Rowland, and M. Wolfsberg (1997), $^{12}C/^{13}C$ kinetic isotope effects in the reactions of CH_4 with OH and Cl 24, *Geophys. Res. Lett.*, *24*, 2761–2764, doi:10.1029/97GL02858.

Hein, R., and P. J. Crutzen (1997), An inverse modeling approach to investigate the global atmospheric methane cycle, *Global Biogeochem. Cycles*, *11*, 43–76, doi:10.1029/96GB03043.

IPCC (2001), *Climate Change 2001 IPCC Third Assessment Report*, Intergovernmental Panel on Climate Change, WMO/UNEP, Wembley, U. K.

IPCC (2013), *Climate Change 2013 IPCC Fifth Assessment Report*, Intergovernmental Panel on Climate Change, WMO/UNEP, Stockholm.

Joelsson, L. M. T., R. Forecast, J. A. Schmidt, C. Meusinger, E. J. K. Nilsson, S. Ono, and M. S. Johnson (2014), Relative rate study of the kinetic isotope effect in the $^{13}CH_3D$ + Cl reaction, *Chem. Phys. Lett.*, *605-606*, 152–157.

Joelsson, L. M. T., J. A. Schmidt, E. J. K. Nilsson, T. Blunier, D. W. T. Griffith, S. Ono, and M. S. Johnson (2016), Kinetic isotope effects of $^{12}CH_3D$ + OH and $^{13}CH_3D$ + OH from 278 to 313 K, *Atmos. Chem. Phys.*, *16*(7), 4439–4449, doi:10.5194/acp-16-4439-2016.

Jones, L. H., and R. S. McDowell (1959), Force constants dynamic of methane, *Functions*, *653*, 632–653.

Kaye, J. A., and C. H. Jackman (1990), Comment on "detection of multiply deuterated methane in the atmosphere", *Geophys. Res. Lett.*, *17*, 659–660, doi:10.1029/GL017i005p00659.

King, S. L., P. D. Quay, and J. M. Lansdown (1989), The ^{13}C /^{12}C kinetic isotope effect for soil oxidation of methane increase, *J. Geophys. Res.*, *94*, 18,273–18,277, doi:10.1029/JD094iD15p18273.

Kirschke, S., et al. (2013), Three decades of global methane sources and sinks, *Nat. Geosci.*, *6*, 813–823.

Krishnan, R., J. S. Binkley, R. Seeger, and J. A. Pople (1980), Self-consistent molecular orbital methods. XX. A basis set for correlated wave functions, *J. Chem. Phys.*, *72*(1), 650–654.

Lasaga, A. C., and G. V. Gibbs (1991), AB Initio studies of the kinetic isotope effect of the CH_4 + OH atmospheric reaction, *Geophys. Res. Lett.*, *18*, 1217–1220.

Lee, T. J., J. M. L. Martin, and P. R. Taylor (1995), An accurate ab initio quartic force field for formaldehyde and its isotopomers, *J. Mol. Spectrosc.*, *160*, 105–116, doi:10.1006/jmsp.1993.1161.

Lelieveld, J., P. J. Crutzen, and F. J. Dentener (1998), Changing concentration, lifetime and climate forcing of atmospheric methane, *Tellus Ser. B Chem. Phys. Meteorol.*, *50*(2), 128–150, doi:10.1034/j.1600-0889.1998.t01-1-00002.x.

Levin, I., P. Bergamaschi, H. Dorr, and D. Trapp (1993), Stable isotopic signature of methane from major sources in Germany, *Chemosphere*, *26*, 161–177.

Liu, Q., and Y. Liu (2016), Clumped-isotope signatures at equilibrium of CH_4, NH_3, H_2O, H_2S and SO_2, *Geochim. Cosmochim. Acta*, *175*, 252–270, doi:10.1016/j.gca.2015.11.040.

Lowe, D. C., W. Allan, M. R. Manning, T. Bromley, D. Ferretti, A. Gomez, R. Knobben, R. Martin, and Z. Mei (1999), Shipboard determinations of the distribution of ^{13}C in atmospheric methane in the Pacific, *J. Geophys. Res.*, *104*, 26,125–26,135, doi:10.1029/1999JD900452.

Ma, Q., S. Wu, and Y. Tang (2008), Formation and abundance of doubly-substituted methane isotopologues ($^{13}CH_3D$) in natural gas systems, *Geochim. Cosmochim. Acta*, *72*(22), 5446–5456, doi:10.1016/j.gca.2008.08.014.

Matsumi, Y., K. Izumi, V. Skorokhodov, M. Kawasaki, and N. Tanaka (1997), Reaction and Quenching of Cl (^2P_j) Atoms in Collisions with Methane and Deuterated Methanes. *J. Phys. Chem. A*, *101*, 1216–1221.

Michelsen, H. A. (2001), Carbon and hydrogen kinetic isotope effects for the reaction of Cl with CH_4: Consolidating chemical kinetics and molecular dynamics measurements, *J. Geophys. Res.*, *106*, 12,267–12,274, doi:10.1029/2000JD900689.

Møller, C., and M. S. Plesset (1934), Note on an approximation treatment for many-electron systems, *Phys. Rev.*, *46*(7), 618–622, doi:10.1103/PhysRev.46.618.

Montzka, S. A., M. Krol, E. Dlugokencky, B. Hall, P. Jöckel, and J. Lelieveld (2011), Small interannual variability of global atmospheric hydroxyl, *Science*, *331*(6013), 67–69, doi:10.1126/science.1197640.

Mroz, E. J., M. Alei, J. H. Cappis, P. R. Guthals, A. S. Mason, and D. J. Rokop (1989), Detection of multiply deuterated methane in the atmosphere, *Geophys. Res. Lett.*, *16*, 677–678, doi:10.1029/GL016i007p00677.

Ono, S., D. T. Wang, D. S. Gruen, B. Sherwood Lollar, M. S. Zahniser, B. J. McManus, and D. D. Nelson (2014), Measurement of a doubly substituted methane isotopologue, $^{13}CH_3D$, by tunable infrared laser direct absorption spectroscopy, *Anal. Chem.*, *86*(13), 6487–6494.

Piasecki, A., A. Sessions, B. Peterson, and J. Eiler (2016), Prediction of equilibrium distributions of isotopologues for methane, ethane and propane using density functional theory, *Geochim. Cosmochim. Acta*, doi:10.1016/j.gca.2016.06.003.

Platt, U., W. Allan, and D. Lowe (2004), Hemispheric average Cl atom concentration from $^{13}C/^{12}C$ ratios in atmospheric methane, *Atmos. Chem. Phys.*, *4*, 2283–2300.

Prather, J. (1990), Tropospheric hydroxyl concentrations and the lifetimes of hydrochlorofluorocarbons (HCFCs), UNEP/WMO Scientific Assessment of Stratospheric Ozone, *WMO* 2.

Prinn, R. G., et al. (2005), Evidence for variability of atmospheric hydroxyl radicals over the past quarter century, *Geophys. Res. Lett.*, *32*, L07809, doi:10.1029/2004GL022228.

Quay, P., E. Dlugokencky, J. Stutsman, D. Wilbur, A. Snover, and T. Brown (1999), The isotopic composition of atmospheric methane, *Global Biogeochem. Cycles*, *13*, 445–461, doi:10.1029/1998GB900006.

Rigby, M., et al. (2008), Renewed growth of atmospheric methane, *Geophys. Res. Lett.*, *35*, L22805, doi:10.1029/2008GL036037.

Roberto-Neto, O., and E. L. Coitin (1998), Dual-level direct dynamics calculations of deuterium and carbon-13 kinetic isotope effects for the reaction Cl + CH4, *J. Phys. Chem. A*, *5639*(98), 4568–4578.

Sander, S. P. (2006), Chemical kinetics and photochemical data for use in atmospheric studies, Evaluation 15 JPL Publ. No. 6–2, 523 pp.

Sauer, F., R. W. Portmann, A. R. Ravishankara, and J. B. Burkholder (2015), Temperature dependence of the Cl atom reaction with deuterated methanes, *J. Phys. Chem. A*, *119*, 4396–4407, doi:10.1021/jp508721h.

Saueressig, G., P. Bergamaschi, J. N. Crowley, H. Fischer, and G. W. Harris (1995), Carbon kinetic isotope effect in the reaction of CH_4 with Cl atoms, *Geophys. Res. Lett.*, *22*, 1225–1228, doi:10.1029/95GL00881.

Saueressig, G., J. N. Crowley, P. Bergamaschi, C. A. M. Brenninkmeijer, and H. Fischer (2001), Carbon 13 and D kinetic isotope effects in the reactions of CH_4 with $O(^1D)$ and OH: New laboratory measurements and their implications for the isotopic composition of stratospheric methane, *J. Geophys. Res.*, *106*, 23,127–23,138, doi:10.1029/2000JD000120.

Saunois, M., et al. (2016), The global methane budget 2000-2012, *Earth Syst. Sci. Data*, *8*, 697–751, doi:10.5194/essd-8-697-2016.

Schimmelmann, A., A. L. Sessions, and M. Mastalerz (2006), Hydrogen isotopic (D/H) composition of organic matter during Diagenesis and thermal maturation, *Annu. Rev. Earth Planet. Sci.*, *34*(1), 501–533, doi:10.1146/annurev.earth.34.031405.125011.

Sellevåg, S. R., G. Nyman, and C. J. Nielsen (2006), Study of the carbon-13 kinetic isotope effects in the Cl and OH reactions of CH_4 and CH_3Cl, *J. Phys. Chem. A*, *110*, 141–152, doi:10.1021/jp048440q.

Sherwood Lollar, B., G. Lacrampe-Couloume, G. F. Slater, J. Ward, D. P. Moser, T. M. Gihring, L. H. Lin, and T. C. Onstott (2006), Unravelling abiogenic and biogenic sources of methane in the Earth's deep subsurface, *Chem. Geol.*, *226*, 328–339, doi:10.1016/j.chemgeo.2005.09.027.

Singh, H. B., A. N. Thakur, Y. E. Chen, and M. Kanakidou (1996), Tetrachloroethylene as an indicator of low Cl atom concentrations in the troposphere, *Geophys. Res. Lett.*, *23*, 1529–1532, doi:10.1029/96GL01368.

Stolper, D. A., et al. (2014a), Formation temperatures of thermogenic and biogenic methane, *Science*, *344*, 1500–1503, doi:10.1126/science.1254509.

Stolper, D. A., A. L. Sessions, A. A. Ferreira, E. V. Santos Neto, A. Schimmelmann, S. S. Shusta, D. L. Valentine, and J. M. Eiler (2014b), Combined ^{13}C-D and D-D clumping in methane: Methods and preliminary results, *Geochim. Cosmochim. Acta*, *126*, 169–191, doi:10.1016/j.gca.2013.10.045.

Stolper, D. A., A. M. Martini, M. Clog, P. M. Douglas, S. S. Shusta, D. L. Valentine, A. L. Sessions, and J. M. Eiler (2015), Distinguishing and understanding thermogenic and biogenic sources of methane using multiply substituted isotopologues, *Geochim. Cosmochim. Acta*, *161*, 219–247, doi:10.1016/j.gca.2015.04.015.

Tanaka, N., Y. T. Xiao, and A. C. Lasaga (1996), Ab initio study on carbon kinetic isotope effect (KIE) in the reaction of CH_4 + Cl center dot, *J. Atmos. Chem.*, *23*(1), 37–49.

Truong, T. N., and D. G. Truhlar (1990), Ab initio transition state theory calculations of the reaction rate for OH + $CH_4 \rightarrow H_2O + CH_3$, *J. Chem. Phys.*, *93*(3), 1761.

Tsuji, K., H. Teshima, H. Sasada, and N. Yoshida (2012), Spectroscopic isotope ratio measurement of doubly-substituted methane, *Spectrochim. Acta, Part A*, *98*, 43–46, doi:10.1016/j.saa.2012.08.028.

Wang, D. T., et al. (2015), Methane cycling. Nonequilibrium clumped isotope signals in microbial methane, *Science*, *348*, 428–431, doi:10.1126/science.aaa4326.

Webb, M. A., and T. F. Miller (2014), Position-specific and clumped stable isotope studies: Comparison of the urey and path-integral approaches for carbon dioxide, nitrous oxide, methane, and propane, *J. Phys. Chem. A*, *118*(2), 467–474, doi:10.1021/jp411134v.

Whiticar, M., and H. Schaefer (2007), Constraining past global tropospheric methane budgets with carbon and hydrogen isotope ratios in ice, *Philos. Trans. Ser. A*, *365*, 1793–1828, doi:10.1098/rsta.2007.2048.

Wallington, T. J., and M. D. Hurley (1992), A kinetic study of the reaction of chlorine atoms with CF_3CHC1_2, *Chem. Phys. Lett.*, *189*, 437–442.

Whitehill, A. R., L. M. T. Joelsson, J. A. Schmidt, D. T. Wang, M. S. Johnson, and S. Ono (2017), Clumped isotope effects during OH and Cl oxidation of methane, *Geochim. Cosmochim. Acta*, *196*, 307–325, doi:10.1016/j.gca.2016.09.012.

Wilmshurst, J. K., and H. J. Bernstein (1957), The infrared spectra of CH_4, CH_3D, CH_2D_2, CD_3H, and CD_4, *Can. J. Chem.*, *35*(3), 226–235, doi:10.1139/v57-034.

Wuebbles, D. J., and K. Hayhoe (2002), Atmospheric methane and global change, *Earth Sci. Rev.*, *57*(3–4), 177–210.

Young, E. D., D. Rumble, P. Freedman, and M. Mills (2016), A large-radius high-mass-resolution multiple-collector isotope ratio mass spectrometer for analysis of rare isotopologues of O_2, N_2, CH_4 and other gases, *Int. J. Mass Spectrom.*, *401*, 1–10, doi:10.1016/j.ijms.2016.01.006.

Young, E. D., et al. (2017), The relative abundances of resolved $^{12}CH_2D_2$ and $^{13}CH_3D$ and mechanisms controlling isotopic bond ordering in abiotic and biotic methane gases, *Geochim. Cosmochim. Acta*, *203*, 235–264, doi:10.1016/j.gca.2016.12.041.

Zhao, Y., and D. G. Truhlar (2008), The M06 suite of density functionals for main group thermochemistry, thermochemical kinetics, noncovalent interactions, excited states, and transition elements: Two new functionals and systematic testing of four M06-class functionals and 12 other function, *Theor. Chem. Acc.*, *120*, 215–241, doi:10.1007/s00214-007-0310-x.